

THE FORMATION OF PLASMA BEAMS CONTAINING IONIC SPECIES

Stanley Singer, N. G. Kim, A. W. Merkl, L. B. Marantz
and C. Bodai

Research and Development Laboratories · RPI

Pasadena, California

The preparation of a plasma from substances stable under ordinary conditions can provide a steady state mixture of many reactive species. Neutral and ionic fragments are formed from the original reagent as a result of the high temperature and electron impact processes. The plasma involves a complex mixture of free radicals and ions in different levels of excitation. The formation of different species at different excitation levels in the plasma presents the possibility of different chemical reactions and products from a single reagent (c.f., for example, ref. 1). A study was made to devise a preparation of relatively pure reagents such as might be found in a plasma. A method in which the identity and excitation level of the reagent could be well known was desired. Ionic species have proven to be effective reagents, particularly in liquid phase organic reactions.

Many ionic species are readily formed by electron impact. The magnetron ion source is particularly suited for the formation of ions in large quantities with low energy electrons.^{2,3} Specific methods have been required for large currents of particular ionic species. For example, a beam of protons has been prepared from hydrogen-saturated titanium by using an electrical discharge along the surface of the metal.⁴ Ions have been made from the alkali metals by thermionic emission from a hot surface with a suitable work function such as tungsten.⁵ The preparation of polyatomic ions has been carried out in ion sources similar to those used in mass spectrometers by electron impact. Electron energies most effective for ionization are used, usually from 70-100 electron volts. Such energies are much greater than the threshold required for ionization of most organic molecules and fragmentation results, providing a mixture of many different ions. The magnetron ion source provides a large current of ionizing electrons at low energies, and the resultant controlled ionization permits formation of plasmas containing selected ionic species.

1. K. R. Kopecky, G. S. Hammond, and P. A. Leermakers, *J. Am. Chem. Soc.* **83**, 2397 (1961).
2. B.G. Perovic, "Proceedings of the Third International Congress on Ionization Phenomena in Gases (Venice, June 1957)," Italian Society of Physics, Milan, October 1957, p. 813.
3. H.R. Kaufman, "An Ion Rocket with an Electron-Bombardment Ion Source, National Aeronautics and Space Administration, Technical Note D-585, Washington D.C., January, 1961.
4. K. W. Ehlers et al., *Rev. Sci. Instr.* **29**, 614 (1958).
5. M. von Ardenne, "Tabellen der Elektronenphysik, Ionenphysik, und Ultramikroskopie," Deutscher Verlag der Wissenschaften, Berlin, 1956, Vol. I, p. 498.

EXPERIMENTAL

A dual-anode magnetron has been used for preparation of the ionic plasmas by electron impact. The usual magnetron configuration was modified, as shown in Fig. 1, by the addition of a central anode. A heated tungsten filament, used as the electron source, is placed between the two anodes also in a cylindrical surface. Electrons falling from this filament to the two anodes are provided with carefully controlled energies by placing the anodes at potentials only slightly above the appearance potential of the ion of interest. A magnetic field of approximately 500 gauss is applied along the axis of the source.

The outer cylinder of this source, which provides a plasma consisting largely of single ionic species and electrons, is a copper tube 7.5 cm. in diameter and 10 cm. in length as shown in Fig. 1. An orifice 1.9 cm. in diameter in the cylinder allows the extraction and study of the ions. The gas to be subjected to electron impact is passed into the magnetron through a 3 mm. tube on the opposite side from this orifice. Copper cooling coils through which water circulates are wrapped around the outside of the cylinder. The central anode is a 1 cm. steel rod. The heated cathode is a tungsten filament 66 cm. in length and 0.76 mm. (0.030 inches) in diameter, and is drawn through insulated supports from one end to the other of the cylinder in alternating strands so as to be midway between the concentric anodes. The tungsten cathode was heated with approximately 30 amperes of 60 volt a.c. current.

In forming the desired plasma the ionizing gas is passed into the source at pressures of 5×10^{-4} to 1×10^{-3} Torr. If the electron energy required to ionize the gas is known, the anodes are placed a few volts above the necessary ionization potential, and the filament temperature is gradually increased until a collector placed a short distance outside the orifice indicates extraction of a strong current. Currents obtained with different anode potentials have been studied. If the ionization energy involved is unknown, the above procedure may be followed to determine effective conditions for generation of the desired plasma. Filament current, gas pressure, and anode potentials all affect ionization of a specific gas strongly, and these parameters interact strongly during operation of the magnetron. The ions formed were identified in this work by mass spectrometric analysis with a radio frequency quadrupole mass spectrometer.⁶ The ionization of three gases was studied in this way, nitrogen dioxide (Matheson, 99.5%), tetrafluorohydrazine (Air Products and Chemical Co., Research Grade, 99+%), and oxygen difluoride (General Chemical Div. of Allied Chemical Co.).

Extraction of the positive ion current when nitrogen dioxide was ionized in the magnetron with anode potentials of 12.5 volts showed that more than 99% of the ions formed were NO_2^+ . Less than 1% of the ions in the extracted current were NO^+ . With increasing anode potentials the amount of NO^+ increased. At 15 volts the beam contained approximately 5% of NO^+ ; and at 30 volts it contained 27% of NO^+ . With tetrafluorohydrazine ionization at anode potentials of 12 volts gave a plasma containing largely NF_2^+ , indicated by mass spectrometric analysis of the extracted ion beam in which 93% of the ions were NF_2^+ . The remaining species were NF^+ , and possibly a small quantity of NO^+ from impurities in the initial material. With increase in anode potentials the quantity of NF^+ in the extracted

6. W. Paul, H. P. Reinhard, and U. Von Zahn, *Z. Phys.* **152**, 143 (1958).

current increased, similar to the effect observed with nitrogen dioxide. Ionization of oxygen difluoride was studied at anode potentials of 13 volts. The only positive ion detected was OF^+ which made up 76% of the ionic current extracted. Fluoride ion was also found; the negative ion was ca. 24% of the total extracted beam.

DISCUSSION

Magnetron Characteristics. - The concentric anode configuration of the magnetron used in these studies results in a markedly different electric field from that in the standard magnetrons. The strong axial magnetic field aids in efficient use of electrons for ionization, necessary in view of the low electric fields present. Ion currents on the order of 1 milliampere can be extracted from the magnetron by potentials of 1 to 10 volts, and if desired the flow of gas into the magnetron can be adjusted so that the extracted current corresponds to almost complete ionization of the entering gas. The anode potentials correspond to the maximum energy available from the ionizing electrons. With energies very close to the appearance potential of the desired ion the cross section for ionization is very low. This obstacle in forming a high concentration of ions is overcome in part by using a large electron current. Under typical operating conditions electron flow of 1 1/2 to 5 amperes to the anodes has been observed. Use of an oscilloscope to observe the currents flowing in the magnetron has shown that large 60-cycle electron pulses flow to the anodes. At typical pressures (0.5 - 1.5 microns) the pulse duration is 1-10 milliseconds; the pulse length increases with increasing pressure. These pulses briefly lower the anode potentials approximately 1/2 volt.

Formation of NO_2^+ Plasma. - Previous studies of the ionization of nitrogen dioxide by electron impact, aside from determinations of the ionization potential, showed that NO^+ was the predominant ion formed when electron energies of 40-70 volts were employed.^{7,8} Although the possibility of forming a plasma containing almost 90% of NO^+ was shown,⁷ NO_2^+ varied from less than 10% to perhaps 20% of the total ionic species, as estimated from the mass spectrometric peak intensities. Monatomic and diatomic positive ions of both nitrogen and oxygen were also present. Eight different ionization potentials varying from 9.78 electron volts up to 18.87 electron volts have been reported for nitrogen dioxide.⁹⁻¹⁵ The higher ionization potentials reported have been attributed to formation of the ion in excited electronic states.

The use of lower energy electrons for ionization in this work evidently prevented formation of significant quantities of NO^+ . Reduction of magnetron anode potentials

-
7. E. G. C. Stueckelberg, and H. D. Smyth, *Phys. Rev.* **36**, 478 (1930).
 8. R. A. Friedel, A. G. Sharkey, Jr., J. L. Schultz and C. R. Howard, *Anal. Chem.* **25**, 1314 (1953).
 9. T. Nakayama, M. Y. Kitamura, and K. Watanabe, *J. Chem. Phys.* **30**, 1180 (1959).
 10. D. C. Frost, D. Mak, and C. A. McDowell, *Can. J. Chem.* **40**, 1064 (1962).
 11. R. J. Kandel, *J. Chem. Phys.* **23**, 84 (1955).
 12. K. Watanabe, *J. Chem. Phys.* **26**, 542 (1957).
 13. W. C. Price and D. M. Simpson, *Trans. Faraday Soc.* **37**, 106 (1941).
 14. J. Collin and F. P. Lossing, *J. Chem. Phys.* **28**, 900 (1958).
 15. Y. Tanaka and A. S. Jursa, *J. Chem. Phys.* **36**, 2493 (1962).

from 12.5 to 11.0 volts gave no further decrease in NO^+ concentration noted in ions extracted. The presence of some 6 reported ionization potentials lying between 9.78 and 12.3 electron volts, however, indicates that several electronic states may be present.

In previous investigations the formation of fragment ions was attributed, at least in part, to thermal dissociation as a result of the hot cathode. The present results show that ionization in the magnetron occurs prior to dissociation and that higher electron energies can cause fragmentation.

Formation of NF_2^+ Plasma. - The use of tetrafluorohydrazine in preparation of the NF_2^+ plasma demonstrates how the ionizing gas can be selected to avoid the formation of undesired ions in certain cases. Ionization of ammonium trifluoride has been reported to give NF_2^+ as the major product.¹⁶ The parent ion, NF_3^+ and the fragment NF^+ were also formed in significant quantities, however. If lower electron energies, slightly above the appearance potential of NF_2^+ from nitrogen trifluoride, were used it appears likely that significant, possibly greater, quantities of NF_3^+ would be formed because of the lower appearance potential of the latter ion and the rapid increase of ionization efficiency with electron energy near the appearance potential. In addition, fluorine atoms or possibly fluoride ions accompany the formation of NF_2^+ from nitrogen trifluoride. The symmetrical structure of tetrafluorohydrazine indicates the possibility of preparation of a plasma containing only NF_2^+ ions. The appearance potentials of ions from tetrafluorohydrazine have been determined, and mass spectroscopic studies have been made showing the ionic composition obtained by ionization with electrons of moderate energy.^{17,18,19,20}

The formation of NF_2^+ with magnetron anode potentials of 12 volts, slightly below the published appearance potentials of this ion from tetrafluorohydrazine, 12.5 to 12.7 volts,^{18,20} may indicate either the spread of electron energies in the magnetron or ionization of NF_2 radicals, which may form by dissociation of parent molecules and which have ionization potential below 12 volts.²⁰

Preparation of OF^+ Plasma. - Mass spectrometric studies of the ionization of oxygen difluoride with 70 volt electrons showed the formation of the parent peak for OF_2^+ in greater quantities than OF^+ .²¹ The appearance potential of OF^+ from the neutral fragment OF was estimated at 13.0 electron volts, from the parent molecule, 15.8 volts. The magnetron anodes were therefore placed at 13 volts, below the appearance potential reported for OF_2^+ , 13.7 volts. Extraction of ion current from the magnetron by means of external potentials and mass spectrometric analysis of the ions showed the presence of OF^+ and no other positive ions. The negative ion F^- was also observed, in quantities less than 1/3 the OF^+ current. Thus, attempts to ionize oxygen difluoride may provide a plasma containing large quantities of fluorine atoms in addition to the OF^+ and F^- ions.

ACKNOWLEDGMENT

The encouragement of Dr. J. F. Masi and the support of the Air Force Office of Scientific Research are gratefully acknowledged.

16. R. M. Reese, and V. H. Dibeler, *J. Chem. Phys.* 24, 1175 (1956).
17. C. B. Colburn and A. Kennedy, *J. Am. Chem. Soc.* 80, 5004 (1958).
18. J. T. Herron and V. H. Dibeler, *J. Chem. Phys.* 33, 1595 (1960).
19. C. B. Colburn and F. A. Johnson, *J. Chem. Phys.* 33, 1869 (1960).
20. A. Kennedy and C. B. Colburn, *J. Chem. Phys.* 35, 1892 (1961).
21. V. H. Dibeler, R. N. Reese and J. L. Franklin, *J. Chem. Phys.* 27, 1296 (1957).

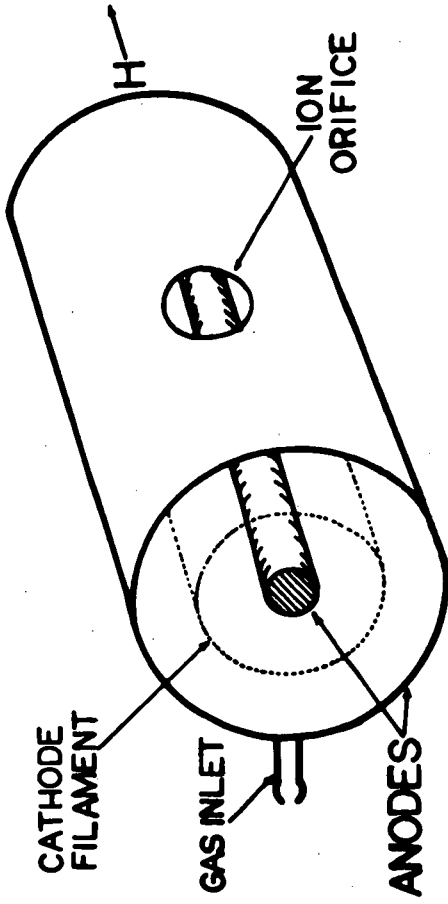


Fig. 1. Concentric Dual-Anode Magnetron

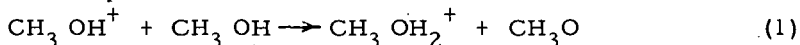
Ion-Molecule Reactions in Methanol and Ethanol

Keith R. Ryan⁽¹⁾, L. Wayne Sieck, and Jean H. Futrell

Aerospace Research Laboratories
Office of Aerospace Research
Wright-Patterson Air Force Base, Ohio

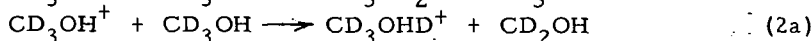
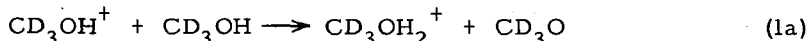
INTRODUCTION

The very large cross section observed for proton transfer ion-molecule reactions in alcohol has prompted a number of workers to investigate these systems in some detail. Theard and Hamill investigated the dependence of the cross section for proton transfer on the field strength in the ion source for 70 volt electrons (1), while Moran and Hamill have shown that the total cross section for these reactions changes significantly with the energy of the ionizing electrons. (2) Recently extensive studies on ethanol and methanol by the method of charge exchange have been reported by Lindholm et al. (3, 4, 5) In addition, these workers determined relative cross sections for the two possible proton transfer reactions between the parent methanol ion and methanol molecules

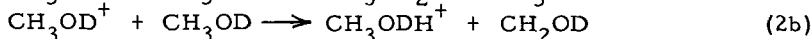


The use of the isotopically labeled methanol (CD_3OH) established the mechanism of formation of the product ion.

In Lindholm's apparatus the secondary ion beam is extracted in a direction perpendicular to the direction of the primary ion beam. This procedure is certainly suitable for the study of dissociative charge transfer but severe discrimination occurs against the extraction of secondary ions formed by processes involving momentum transfer. This discrimination is sufficient to preclude the observation of ion-molecule interactions in which entities other than the isotopes of hydrogen are transferred. Furthermore, in the reactions



the observed relative rate constants will be greater than for the equivalent reactions in methanol because of both this discrimination and the deuterium isotope effect. An indication of the magnitude of these effects can be obtained from the parallel reactions with CH_3OD



which have also been reported by Lindholm and Wilmenius. (5)

An examination of recorded appearance potential data for methanol reveals that at least one volt separates the onset of the parent ion and the process of next lowest energy (6). Consequently a study of proton transfer in the electron energy region below the onset of the CH_2OH^+ ion should yield information on the required

(1) Visiting Research Associate

cross sections. Once these are known a study of proton transfer as a function of electron energy should allow the elucidation of additional proton transfer reactions in the methanol system. These results, using the older techniques of ion molecule studies, are essentially free of momentum discrimination effects.

Until now the proton transfer reaction in ethanol has been assumed to involve the parent ion exclusively (7). By analogy with methanol it appeared that this reaction might also occur with the $\text{CH}_3\text{CH}_2\text{OH}^+$ ion. Accordingly an examination of the possible proton transfer reactions in ethanol was also undertaken.

Experimental

The instrument used in this study, a modified Consolidated Model 21-103C, has been described recently (8). The Bendix model M.306 electron multiplier was replaced by a Consolidated electron multiplier while the Wien filter was retained.

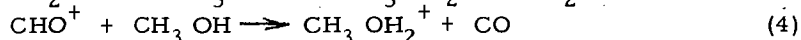
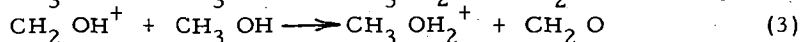
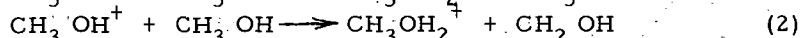
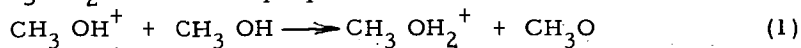
Appearance potentials were measured in the following manner: Magnetic scanning was used to bring the ions of interest to focus at 500 volts. Electric fields in the ionization region were reduced by operating the electron trap at 10 volts and both ion repellers at 4.5 volts. In order to compare the appearance potentials of two ions the sensitivity of the ion detector was adjusted so that the apparent abundances of both ions were the same at 50 electron volts. The appearance potential of an ion was arbitrarily taken to be the electron energy at which the ion current had fallen to 0.3 per cent of its value at 50 electron volts. Because of the similarity in shape of the curves being compared this technique was considered to be satisfactory. Furthermore, the difference in appearance potential between any two ions studied was constant irrespective of whether of the onset was chosen as the energy where the ion current had reached 0.1, 0.2 or 0.3 per cent of its value at 50 volts. In subsequent sections of this paper we are concerned only with the difference in energy for the onset of several processes. Accordingly we have used an uncorrected electron energy scale.

To facilitate the determination of appearance potentials, the ionization efficiency curves were displayed directly on an Electro Instrument Inc. model 300 X-Y recorder. Since the ion source of the mass spectrometer is always at acceleration potential (relative to ground) a signal from the helipot used to control the electron energy could not be fed directly to the recorder. Accordingly the output of the electron energy helipot was transmitted mechanically by means of an insulating shaft to a second helipot. A constant one volt signal was placed across this second potentiometer causing an electrical signal proportional to the electron energy to be developed between one end of the helipot and the moving contact. This signal was transmitted to the recorder and, suitably attenuated, was applied to the x-axis.

The relationship between reservoir pressure and ion source concentration was determined after the method described by Stevenson and Schissler, (9) using the ionization cross section of argon and the dimensions of the source. In this calibration reservoir pressures were read directly from the micromanometer provided with the instrument. In the methanol investigation reservoir pressures greater than 584 microns were sometimes employed. Since this pressure is the upper limit of reading of the micromanometer range all ion source concentrations corresponding to higher reservoir pressures than this were measured directly in the source by the method of total ionization. To convert total ion current to units of concentration it is only necessary to know the ionization cross section of methanol relative to argon. This was determined at lower ion source concentrations where the reservoir pressures of the gases could be measured.

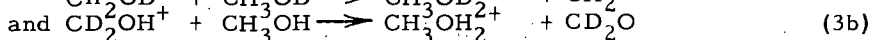
Formation of $\text{CH}_3\text{CH}_2\text{OH}_2^+$

The CH_3OH_2^+ ion has been observed in the high pressure mass spectrum of methanol, (1, 2, 9, 10) in the mass spectrum of mixtures of methanol and water (11) and in the experiments of Lindholm et al. (3-5) Mechanisms for the formation of CH_3OH_2^+ have been proposed as follows:



Using isotopically substituted methanols Theard and Hamill (1) found the appearance potentials for mechanisms (1) and (2) to be the same within experimental error.

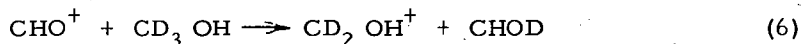
The importance of reaction (3) involving proton transfer from the hydroxyl position has been demonstrated by Lindholm and Wilmenius (5), who observed the reactions



in their tandem instrument. They also postulated mechanism (4) followed by the subsequent dissociation of some of the product ion (2)

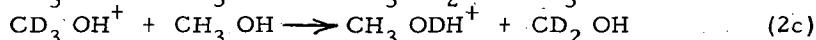
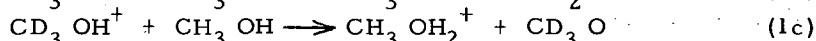
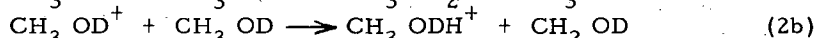
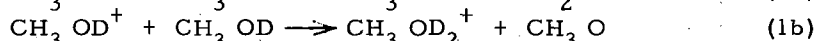
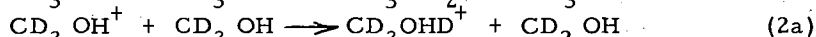
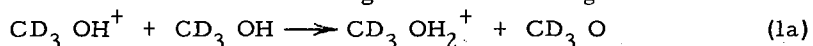


However, in a later publication (3) the same authors appear to favor the following hydride ion transfer reaction



over reaction (4).

In order to determine the relative cross sections of reactions (1) and (2) Lindholm and Wilmenius investigated the following reactions



In these three sets of reactions the ratios of product ion by mechanism (1) to product ion by mechanism (2) were 2:3, 1:3 and 2:3 respectively.

We have studied proton transfer using the techniques outlined by Lampe, Franklin and Field. (12) Since in our ion source secondary ions formed along the path of the primary ion beam are extracted in the same direction as the primary ion beam, discrimination because of momentum transfer should be minimized.

Figure 1 shows a plot of $\frac{\text{CD}_3\text{OH}_2^+}{\text{CD}_3\text{ODH}^+}$

against nominal electron energy over an eight volt range near threshold in the high pressure mass spectrum of CD_3OH . The curve has three distinct regions; A.

and C. In the low energy region one can detect only those secondary ions which have the parent ion as their precursor. As the electron energy is increased the curve breaks steadily upward along B. This is interpreted as the appearance of $CD_3OH_2^+$ ions from reaction of CD_2OH^+ with CD_3OH analogous to reaction (3). Eventually an electron energy is reached above which the ratio of product of CD_3CHD^+ relative to the rate of production of $CD_3OH_2^+$ is again constant. The establishment of this plateau C demonstrates that the only two ions which contribute significantly to proton transfer in this region of electron energy are CD_3OH^+ and CD_2OH^+ . It may be noted that this second plateau occurs in the same region of nominal ionizing voltage where the ionization efficiency curves for CH_2OH^+ and CH_3OH^+ from methanol are parallel.

The mean ratio in the plateau region A is about 0.92:1 whereas the ratio in the second plateau region is approximately 1.75:1. A parallel set of measurements using CH_3OD resulted in a value of 0.71 for the ratio $\frac{CH_3OD_2^+}{CH_3ODH^+}$ in plateau region A.

Under the source conditions employed it is apparent that the ratio of product from reaction (1) to product from reaction (2) must lie between 0.92:1 and 0.71:1. In order to estimate the true ratio one may proceed as follows: Let α be the ratio of the probability of transferring H^+ to that of transferring D^+ from any position on the molecule. Further let β be the ratio of the probability of collecting an ion to which H^+ been transferred to that of collecting an ion to which D^+ has been transferred. Clearly β is a measure of the momentum discrimination against D^+ transfer. If R is the true ratio for the transfer then

$$R = \frac{0.92}{\alpha\beta} \quad \text{from reactions 1a and 2a.}$$

$$R = 0.71 \alpha \beta \quad \text{from reactions 1b and 2b.}$$

Hence, $\beta = 1.14$ and a value of $R = 0.81$ may be deduced from our measurements.

Similar treatment of the results of Lindholm and Wilmenius gives $\beta' = 1.4$ and $R = .475$. If we assume α to be the same in both sets of results one obtains $\beta' = 1.24$. This leads to the expected result that discrimination against momentum transfer is considerably greater in the collision chamber used by Lindholm and Wilmenius.

It is not clear why the values of R calculated from our results and those of Lindholm and Wilmenius should be so different. One experimental uncertainty is the energy of the impacting ion beam. Since it is well known that cross sections for ion-molecule reactions are strongly dependent on the velocities of the primary ions, the measured ratio may depend on the ion velocity. Lindholm and Wilmenius report their measurements for ions of about 5 e.v. impacting energy. Our results in Figure 1 are reported for a repeller value of 4.5 volts. The geometry of the C. E. C. 103 ion source is such that the maximum energy an ion can acquire before arriving at the ion exit slit is about half the repeller voltage. This maximum energy of about 2.3 volts is somewhat lower than the energy of the ions used by Lindholm. However, we found no significant change in the measured ratio when the field strength was varied from 4 to 40 volts/cm. From our results we therefore, conclude that the relative probability of proton transfer from the two positions is independent of ion energy over this range.

From the results of Theard and Hamill (4) in their study with CD_3OH it is clear that the ratio $\frac{CD_3OH_2^+}{CD_3ODH^+}$ at an electron impacting energy of 70 volts remained

unchanged as the field strength was varied from 12 to 80 volts/cm. Since this ratio reflects the contribution of several independent proton transfer processes it can be assumed that the ratio of the reaction rates of any two of these processes is independent of field strength.

Once the ratio of proton transfer from reactions (1) and (2) is established the relative importance of processes such as (3) and (4) at higher electron energies can be determined. As shown in Table 1 the ratio $\frac{CD_3ODH^+}{CD_3OH^+}$ is independent of

electron energy for some seven volts above the ionization potential. Combining this result with the fact that the ratio $\frac{CD_3OH_2^+}{CD_3OHD^+}$ from reactions involving the parent

ion is 0.92:1 it is possible to calculate the amount of $CD_3OH_2^+$ formed by reactions involving ions other than the parent ion. Also shown in Table 1 is the ratio $\frac{\Delta CD_3OH_2^+}{CD_2OH^+}$ where $\Delta CD_3OH_2^+$ represents the increase in $CD_3OH_2^+$ due to ions

other than the parent. Because $\frac{\Delta CD_3OH_2^+}{CD_2OH^+}$ is constant for at least 10 volts above the onset of CD_2OH^+ we conclude that CD_2OH^+ is the only ion apart from the parent ion which contributes significantly to the formation of $CD_3OH_2^+$ in this energy range. The increase at 14 volts indicates the onset of additional deuteron transfer processes.

As would be expected, the formation of $CH_3OH_2^+$ from methanol by processes not involving the parent ion is reflected in the appearance potential curve of the secondary ion. We have already mentioned the appearance potentials were obtained by comparing the ionization efficiency curves for two ions after arbitrarily making their sensitivities equal at 50 electron volts. However, this procedure is only satisfactory when each of the ions is formed by only one process. When more than one process contributes to the formation of a given ion this fact must be considered. This is illustrated in Figure 2. In 2a we compare the ionization efficiency curves of CH_3OH^+ with $CH_3OH_2^+$ by adjusting the ion detector to indicate equal sensitivities for both ions at 50 electron volts. It can be seen that the apparent onset of $CH_3OH_2^+$ is higher than the onset of CH_3OH^+ .

In Figure 2b we again compare the ionization efficiency curve of $CH_3OH_2^+$ with that of CH_3OH^+ . In this case we have taken into account the observation that only 46% of the $CH_3OH_2^+$ ions are formed from the parent ion when making the sensitivity adjustment at 50 electron volts. When this is done it can be seen that both ions have the same apparent onset. The upward break in the $CH_3OH_2^+$ curve corresponds to the formation of significant amounts of $CH_3OH_2^+$ from CH_2OH^+ .

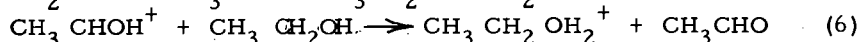
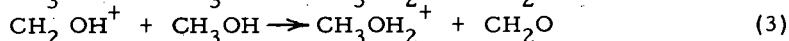
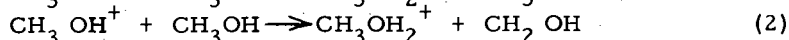
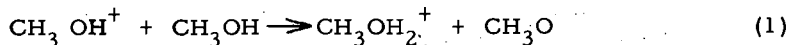
Formation of $C_2H_5OH_2^+$ in Ethanol

Several workers have observed the formation of $C_2H_5OH_2^+$ in the high pressure mass spectrum of ethanol. Tal'roze compared the appearance potential curves of $C_2H_5OH_2^+$ and $C_2H_5OH^+$ and concluded that $C_2H_5OH^+$ was a precursor for the formation of $C_2H_5OH_2^+$. (7) No other ions have previously been associated with the formation of $C_2H_5OH_2^+$.

In Figure 3 we show our ionization efficiency curves for the ions CH_3CHOH^+ , $\text{CH}_3\text{CH}_2\text{OH}^+$ and $\text{CH}_3\text{CH}_2\text{OH}_2^+$. From these results it is clear that CH_3CHOH^+ is the only important precursor for the formation of $\text{CH}_3\text{CH}_2\text{OH}_2^+$ for at least ten volts above the onset of $\text{CH}_3\text{CH}_2\text{OH}^+$. Furthermore, the same cross section is obtained for this reaction in the energy range of Figure 3 and at 70 ev. In sharp contrast to methanol the ethanol molecular ion plays no significant part in the formation of $\text{CH}_3\text{CH}_2\text{OH}_2^+$. This difference between the two molecules does not seem explicable in terms of the energetics of the corresponding reactions. Tal'roze and Frankevich have established lower limits and tentative upper limits to the proton affinities of the alcohols as 177-183 kcal/mole for methanol and 185-202 kcal/mole for ethanol. (11) From the work of D'or and Collin (12) and tabulated heats of formation in Field and Franklin (6) one can estimate the proton affinity of the methanol radical CH_2OH as 153 kcal/mole and of the ethanol radical CH_3CHOH as 159 kcal/mole. We are unable to suggest an alternate explanation.

Rate Constants for Proton Transfer Reactions

Having established the relative rates of proton transfer in the case of methanol and having shown that CH_3CHOH^+ , not $\text{CH}_3\text{CH}_2\text{OH}^+$, is the precursor for $\text{CH}_3\text{CH}_2\text{OH}_2^+$ formation it is possible to determine the rate constants for the following reactions



Consistent with recently tabulated values (13) we have determined rate constants and reaction cross sections at an ion repeller field of 10 volts/cm. Rate constants for all these reactions were observed to rise sharply at low field strength and to decrease at higher values, as is normally observed for ion-molecule reactions involving complex molecules. However, no attempt to extrapolate these results to zero field strength in order to obtain rate constants for thermal ions has been made.

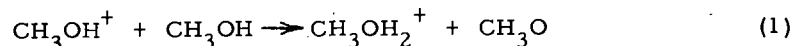
For any given secondary reaction, a plot of the ratio of secondary ions to the sum of precursor ions and secondary ions against ion source concentration is a straight line. As shown by Lampe and Field the slope S of this line can be expressed as

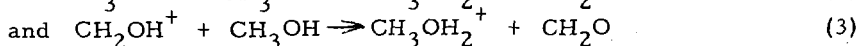
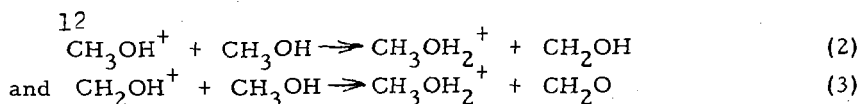
$$S = k\tau \quad (a)$$

$$S = l\sigma \quad (b)$$

Where k is the specific reaction rate, τ is the source residence time of the primary ion, l is the path length from the point of formation of the primary ions to the ion exit slit and σ is the reaction cross section. (14)

Reported in Table 2 are the reaction cross sections and rate constants for the reactions discussed. Also shown are results for methane from this study compared with earlier work. In this compilation we have corrected for the observation that 71% of the proton transfer product ion at a nominal electron impacting energy of 15 electron volts is produced by the parent ion. Since at this energy the remaining 29% of proton transfer product can be attributed to the CH_2OH^+ ion, the rate constants for

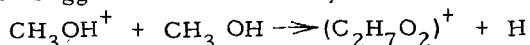




can be calculated by measuring the amount of proton transfer product at 15 volts and using the observed relative rates of reactions (1) and (2).

Ions with higher mass-to-charge ratios than those involving proton transfer

During this study we observed ions in the high pressure mass spectra of methanol and ethanol that had masses greater than those corresponding to proton transfer. In methanol the ions 73, 72, 63 and 45 were all observed. Of these only the 63 ion consistently exhibited a square law dependence on pressure. We are not sure of the mechanism of formation of these ions, but it is clear that 73 and 72 cannot be formed by second order ion molecule reactions involving only pure methanol. The appearance potential for 63 agrees well with that for CH_3OH^+ which suggests it is formed by the reaction.



In any event the abundance of these ions is less than 0.5 per cent of those produced by proton transfer.

In the high pressure mass spectrum of ethanol ions of mass-to-charge ratio 77 and 73 were both observed to follow a square law dependence with pressure. The relative abundance of these ions was less than 0.5 per cent of the secondary ions produced by proton transfer.

References

1. Theard, L. P. and Hamill, W. H., J. Amer. Chem. Soc. 84, 1134, (1962).
2. Moran, T. F. and Hamill, W. H., J. Chem. Phys. 39, 1413, (1963).
3. von Koch, H. and Lindholm, E., Arkiv For Fysik 19, 123, (1961).
4. Wilmenius, P. and Lindholm, E., Arkiv For Fysik 21, 97, (1962).
5. Lindholm, E. and Wilmenius, P., Arkiv For Kimi 20, 255, (1963).
6. Field, F. H. and Franklin, J. F., "Electron Impact Phenomena and the Properties of Gaseous Ions", Academic Press Inc., New York (1957).
7. Tal'roze, V. L., Pure and Appl. Chem. 5, 455, (1962).
8. Futrell, J. H. and Tiernan, T. O., J. Chem. Phys. 39, 2539, (1963).
9. Schissler, D. O. and Stevenson, D. P., J. Chem. Phys. 24, 926, (1956).
10. Stevenson, D. P., J. Phys. Chem. 61, 1453, (1957).
11. Tal'roze, V. L. and Frankevich, J., J. Amer. Chem. Soc. 80, 2344, (1958).
12. D'Or, L. and Collin, J., Bull. Roy. Soc. Liege 22, 285, (1956).
13. Lampe, F. W., Franklin, J. L. and Field, F. H., "Progress in Reaction Kinetics", G. Porter Ed. Pergamon Press 1961, pages 67 ff.
14. Lampe, F. W. and Field, F. H., Tetrahedron 7, 189, (1959).

TABLE 1

Nominal Energy E.V.	$\frac{CD_3ODH^+}{CD_3OH^+}$	$\frac{CD_3OH_2^+}{CD_2OH^+}$
5.6	.15	
6.0	.15	
6.4	.15	
6.8	.16	
7.2	.16	0
7.6	.16	0
8.0	.16	.08
8.4	.16	.12
8.8	.16	.14
9.2	.16	.14
9.6	.16	.13
10.0	.16	.14
10.4	.16	.13
10.8	.16	.14
12.0	.16	.14
13.0	.16	.14
14.0	.17	.14
15.0	.18	.132

TABLE 2

Reaction	σ , cm ² molecule ⁻¹ x 10 ¹⁶	k, cm ³ sec ⁻¹ molecule ⁻¹ x 10 ¹⁰
CH ₃ OH ⁺ + CH ₃ OH → CH ₃ OH ₂ ⁺ + CH ₃ O	79	11.0
CH ₃ OH ⁺ + CH ₃ OH → CH ₃ OH ₂ ⁺ + CH ₂ OH	97	13.5
CH ₂ OH ⁺ + CH ₃ OH → CH ₃ OH ₂ ⁺ + CH ₂ O	48	6.8
CH ₃ CHOH ⁺ + CH ₃ CH ₂ OH → CH ₃ CH ₂ OH ₂ ⁺ + CH ₃ CHO	531	60
CH ₄ ⁺ + CH ₄ ⁺ → CH ₅ ⁺ + CH ₃	{ 54	10.7
	{ 61 (a)	8.5 (a)

(a) Field, F. H., Franklin, J. L. and Lampe, F. W., J. Amer. Chem. Soc. 79, 2419, (1957)

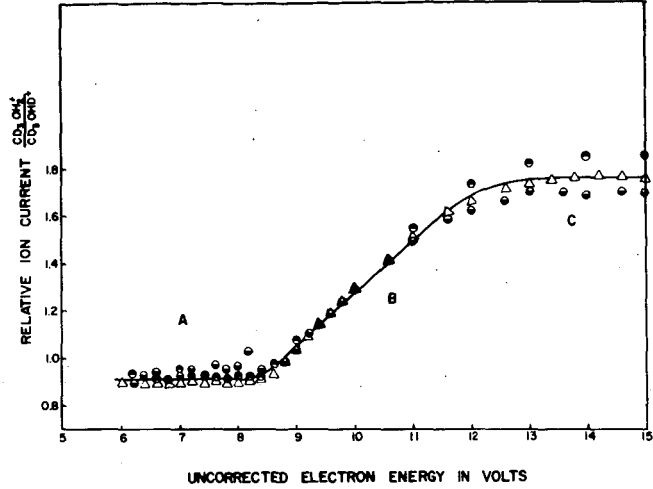


FIGURE 1 $\frac{CD_3OH_2^+}{CD_3OHD^+}$ current versus uncorrected electron energy (3 expts. at 3 different pressures in 3 different sources).

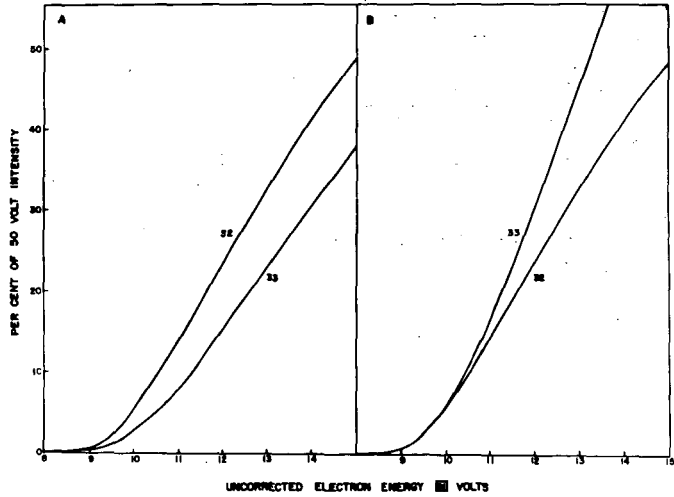
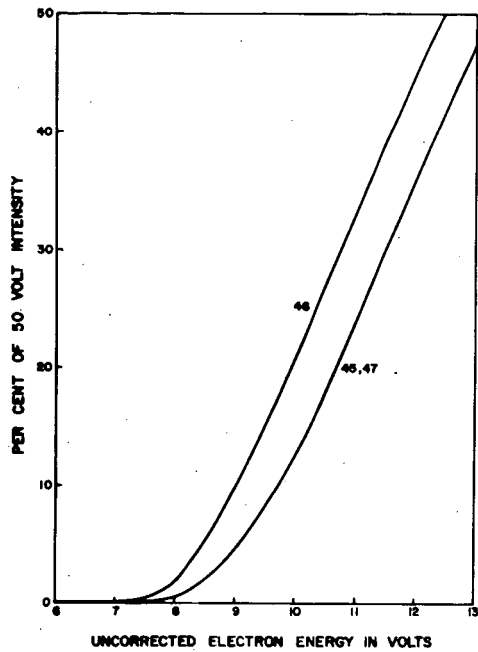


FIGURE 2 Uncorrected ionization efficiency curves for m/e 32 and 33 from methanol normalized to 50 volts and same curves corrected for $CH_3OH_2^+$ from CH_2OH^+ , respectively.



Normalized ionization efficiency curves for m/e 45, 46, and 47 from ethanol.

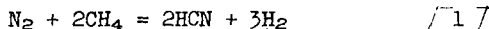
FIGURE 3

THE NATURE AND QUANTITATIVE DETERMINATION OF THE
REACTIVE SPECIES IN A NITROGEN PLASMA JET

Mark P. Freeman
Central Research Division
American Cyanamid Company
Stamford, Connecticut

INTRODUCTION

One of the "natural" reactions found to proceed in a plasma-jet reactor is the formation of hydrocyanic acid by the introduction of methane into a nitrogen jet:



The reaction can be made to proceed in good yield (based on methane consumption) and, furthermore, the main by-products, acetylene and hydrogen, are of considerable chemical significance. This reaction therefore, has received more than passing interest from various investigators purely as a production possibility.

In an ever widening circle of plasma-jet applications this reaction is almost unique in that it is almost certain that the chemistry must proceed via thermally produced intermediate species of a sort unknown at ordinary temperatures. This is the interesting sort of process one would like to contemplate when considering possibilities for plasma jet chemistry. One feels that if insight can be gained into the detailed mechanism for this key reaction, then it is quite possible that avenues will open to exploit other high temperature species in chemical synthesis or, indeed, to use the active species of a nitrogen jet in other reactions.

In the "active nitrogen" research (1,2,3) that has persisted in vigorous

-
- (1) K. R. Jennings and J. W. Linnett, *Quart. Rev.* 12, 116 (1958).
 (2) G. G. Mannella, *Chem. Rev.* 63, 1 (1963).
 (3) N. E. V. Evans, G. R. Freeman and C. A. Winkler, *Can. J. Chem.* 34, 1271 (1956).

activity for more than half a century, HCN plays an equally important role. In fact when cold methane is added to nitrogen at low pressure that has been recently passed through a high-voltage electric discharge, one gets exactly the stoichiometry of [1]. That the experimental systems themselves are different is apparent for the high-voltage discharge is a high-excitation device whereas the plasma jet is thought to be nearly in thermal equilibrium and hence a low-excitation device (spectroscopically speaking)

-
- (4) F. A. Kovolev and Yu. K. Kvaratskheli, *Optics & Spectroscopy*, 10, 200 (1961).

intermediate between arc and spark). Furthermore the plasma jet experiments reported here were performed at one-half atmosphere (as opposed to ~1 torr) and at a temperature twenty times as high on the absolute scale as room temperature, where the bulk of active nitrogen experiments have been performed. Finally, the reactive carbon-containing species evidently does not contact the active nitrogenous species as methane. That is, the products other than HCN are mainly acetylene and higher acetylenes with various degrees of saturation. These are the same products that would form if the jet were, say, argon. It has been shown elsewhere (5) that the precursors

(5) M. P. Freeman and J. F. Skrivan, *AIChE Journal*, 8, 450 (1962).

For these products form rapidly compared to the time for mixing of the methane with the jet.

In spite of these differences it nevertheless does not seem reasonable to say the two systems are only superficially related for the chemistry seems too specific and unique to permit one to accept this interpretation lightly. If one is willing to accept the fact of the chemistry given in equation [1] ... perhaps modified by an asterisk to indicate the nitrogen has been subjected to an excitation of some kind ... as an operational definition for active nitrogen then this study is in a true sense a study of active nitrogen. It is true that the plasma jet provides a difficult environment in which to do precise work. On the other hand this difficulty would seem to be offset by the fact that the relative concentration of active species is observed to be as high as 12% which is two orders of magnitude higher than the (at most) tenths of a percent quoted in conventional research (6).

(6) J. M. Benson, *J. App. Phys.* 23, 759 (1952).

Furthermore, whereas in conventional research on active nitrogen the partial pressure of the active species itself is on the order of hundredths of a torr, it is here observed to be in the tens of torrs. Naturally, this high concentration promotes a considerable simplification in the recovery and analysis of products. Perhaps most significant is the fact that owing to the high temperatures available in a plasma jet atomic nitrogen can be produced in large amount as an equilibrium constituent of the stream and hence serves as an important new variable.

The procedure followed was to add methane through an annular slot to a confined nitrogen jet of precisely defined average enthalpy. It has been shown that under these conditions mixing is very rapid as is the drop in temperature (5). After about 1 millisecond the resulting flow of high temperature species was further chilled by the entrainment of cold product gas .. (the fastest quench known) ... and the flow of HCN in the product gas relative to the effluent nitrogen flow chemically determined. Data were taken at about 350 torr reactor pressure in two reactors that differed in a significant way. In one reactor the methane mixes with the jet as it emerges from the head into a water cooled channel the same size as the front electrode orifice. In the other reactor, the jet enters a plenum chamber, with an exit orifice, and then expands to more than twice the original diameter. Only after the jet has persisted outside the head for more than a millisecond, during which it has lost about half of its enthalpy, is the methane added.

As the methane is added at various flow rates the corresponding rate of production of HCN relative to the effluent nitrogen flow is noted. Just as in Winkler's (7) work with active nitrogen, a plateau is observed which indicates that some active species is indeed determined. Because of equipment availability work was done with the second of the two reactors described above several months in advance of the first, a reactor that is both hotter and more amenable to an enthalpy-dependence study. Because the data from the earlier study indicated an HCN flow rate within a factor two of the nitrogen atom flow rate for a nitrogen stream of enthalpy equal to the average enthalpy (7) it was tentatively concluded (8) that the reagent

(7) F. Martinek, *Thermodynamic and Transport Properties of Gases, Liquid and Solids* (McGraw-Hill, New York, 1959), p. 130.

(8) H. M. Hulburt and M. P. Freeman, *Trans. N. Y. Acad. Sci.*, II, 25, 770 (1963).

species is the nitrogen atom. It is clear from the more complete study reported here

that this conclusion is, in fact, erroneous and that the apparent agreement was fortuitous, a consequence of the choice of power level used in that part of the study.

In order not to confuse what is observed with the immediately apparent interpretation, these factors are separated in the following presentation: After a reasonably complete presentation of the experimental procedure and details (EXPERIMENTAL) sample data are presented together with such generalizations about the data as seem warranted from simple inspection (RESULTS). Following this section, an attempt is made to discuss each of the observations in terms of the various interpretations they would seem to warrant (DISCUSSION). Included in this section is a brief discussion of the principal questions remaining unresolved. Finally, (SUMMARY) those interpretations that would seem most probable are collected together to present a plausible sequence for the observed reaction.

EXPERIMENTAL

Apparatus. Plasma-jet reactors consist of three parts, head or arc unit, intermediate section, and quenching section. The plasma-jet head used for this study is a Thermal-Dynamics L-40 Plasma-jet with "turbulent nitrogen" electrodes and it is powered by two 12 kw welding power supplies open circuit voltage 160 volts connected with their outputs in parallel, but with opposite phase rotations on the input so as to minimize power supply ripple in the output. The intermediate sections (Figures 1 and 2) are made of copper and fully water-cooled as is the head. The SOR (local designation) shown in Figure 2 has ducts and thermometers located so that heat lost to the cooling water upstream of the slot is determined independently from that lost downstream. The quenching section where the hot stream of plasma and reaction products is quenched by entrainment of cold product gas is simply a heat exchanger, i.e., it is a stainless steel pot 11 inches in diameter and 11 inches long sparsely wound with soldered copper tubing. Between the windings it gets hot enough to cause flesh burns but all parts subject to heat damage, such as seals, are well cooled. At the outlet of the quenching section is six feet of 1 inch I.D. thick-walled rubberized fabric acid tubing. This in turn is attached to the bottom of a 3 foot vertical mixing section of 2 inch stainless steel tubing loosely packed with glass wool. At the bottom of this mixing section carbon dioxide is mixed with the now cold discharge from the plasma-jet reactor. The top of the mixing section is connected to a high capacity steam jet vacuum pump with an automatic controller for maintaining desired pressures.

A Toeppler pump is arranged to withdraw 522 ml. of gas from the top of the mixing section at room temperature and at the reactor pressure. This aliquot may then be collected for analysis in a suitable gas collection system.

Gas flows, except for methane, are metered by orifice gages calibrated to within 1% for CO_2 and N_2 respectively by water displacement. Methane flow, much less critical, is determined by a rotameter calibrated by calculation. All cooling water flows are determined by experimentally calibrated rotameters. Cooling water temperature rise is determined by suitably graduated interconsistent mercury thermometers.

Procedure. Heat flow in the nitrogen plasma at the point of methane introduction is determined by subtracting from the voltage-current product in the arc the heat lost to all cooling-water supplies up to that point. (In the case of the TR reactor, a local designation for the reactor configuration of Figure 1, this is just the head cooling water.) For data taken at a particular heat flow (and hence average enthalpy) an attempt was made to keep this heat flow constant. In this endeavor the relatively great intrinsic stability of plasma jets made by this manufacturer

helped, but because data for a typical run extended over several hours there was an appreciable drift with occasional overcorrection (about 15%). This is undoubtedly the principal source of scatter in the data; note that the methane flow rates were set in random order so that trends in the data due to net power drift would not be observed except as scatter.

Except where noted, in all systems the pressure at the sampling tap (called reactor pressure was 350 ± 20 torr. The actual pressure of each sample was known to ± 1 torr but this is not a significant datum in the data analysis. Reactor pressure does not directly measure pressure in the head because of the pressure drop through the arc, which is quite large when the head is operating. Although this unit is not instrumented for an in-head static pressure measurement, some exploratory pressure measurements were run with a tap at the inlet to the head. It was found that pressure changes at this point at the standard flow rate were fairly insensitive to power level, as well as to reactor pressure in the range covered in these experiments. At 350 torr with a gas flow of $0.0171 \text{ gm. mole sec.}^{-1}$ the inlet pressure was observed to be 710 torr. No condition realized in this experiment at this flow rate altered this pressure by more than 10%. Lowering the gas flow rate by 27% reduced the pressure to about 600 torr, a change still less than 20%.

Whenever methane, power and/or pressure conditions were changed the system was operated for eight minutes before taking a sample. This was found to be sufficient time to establish a constant composition.

The collected gas aliquot was slowly sparged through 100 ml. of ice-cold caustic containing 12.50 millimoles of base. The half-liter space over the caustic was initially evacuated so that the entire sample, together with the air used to flush out residual product gas from the lines, might be collected in the caustic and the space over it. This was followed by one minute of vigorous shaking. This procedure has been found satisfactory for the quantitative recovery of CO_2 and HCN. Total acid in the aqueous solution was then determined by titration with 0.500 N HCl until all of the carbonate had been converted to bicarbonate (pH 8.3). Ammoniacal KI was then added as an indicator and cyanide determined alone by precipitometric titration with 0.0100 N silver ion. This permits the initial ratio of partial pressures and hence relative flow rates of HCN and CO_2 to be determined. But the ratio of the flow rates of N_2 (effluent) and CO_2 is known both from the calibrated gages and to similar precision from titration of a blank run done without power or methane. Consequently the ratio of HCN to effluent N_2 follows immediately.

Accounting for the various sources of uncertainty the actual ratio of HCN to N_2 is estimated to be within about 10% of the reported value and the heat flow to within about 5%. Air leakage into the system, a potential source of error, was between 0.1 and 0.01% of the total gas flow.

The quenching section is mounted with a window through which, for a time after each cleaning, the exhaust of the intermediate section can be observed. Under some conditions (notably high enthalpy and low gas flows) rapid solids formation occurred leading, indeed, to plugging at the highest heat flow. It is, therefore, of some interest that when totaled over all runs an inconsequential amount of solid product formed. More than 3 Kg of methane was used in the course of these experiments, resulting in less than 6 g. of recovered solid. This very bulky solid was found on Kjeldahl analysis to contain about 5% nitrogen by weight; it is apparently a mixture of HCN polymer and carbon.

Although temperatures are not quoted (and as will be shown below, cannot be meaningfully quoted because of a substantial departure from equilibrium) it is instructive to note that the eight-fold range of average enthalpy covered in this experiment,

would, on the assumption of equilibrium, correspond to temperatures from 3250°K. to 7000°K.

RESULTS

Yield. In Figure 3 typical results for the yield of hydrocyanic acid as a function of methane feed rate is shown for the TR reactor at a nitrogen flow of 0.0171 g. mole sec.⁻¹, at three widely different enthalpy levels. Several important observations may be made immediately:

- a. At every enthalpy level a limiting value of HCN production is achieved, as observed by Winkler, et al. (3)
- b. After the limiting or saturation value is reached a further excess of methane does not decrease the yield, suggesting a condition of frozen equilibrium.
- c. Before saturation is reached all of the yield curves coincide with each other and with a line slope of 1/3. That is when insufficient methane is added to reach the limiting production, only one carbon atom in three is converted to HCN.

The thing that strikes the investigator is the stability and reproducibility of these effects despite the difficulties inherent in keeping a plasma-jet system operating at precisely defined conditions for several hours. Figure 4 shows a yield curve as in Figure 3 for the highest enthalpy run done in the TR reactor at substantially reduced gas flow. Although this run was plagued by plugging and unstable operation it is clear that no qualitative difference in behavior is to be observed. Also shown in this figure is the initial run done in the SOR reactor at a single enthalpy. Again, essentially the same behavior occurs.

Variation with enthalpy. Because the yield varies rapidly with enthalpy, the enthalpy variations encountered during runs of several hours duration make average values determined from full yield curves such as those of Figures 3 and 4 no more precise than single points using methane flows corresponding to the plateau regions of the curve. At all available enthalpy levels a methane flow rate equal to one-half the nitrogen flow is seen to give the limiting yield of HCN and much of the data describing enthalpy dependence was taken at this feed ratio.

In Figure 5 the logarithm of the flow rate of active species (as measured by the saturation HCN production) is plotted vs reciprocal enthalpy. The open points represent "one point" data; the filled points were determined by a full yield curve of the sort shown in Figure 3. Circular points represent data from the TR reactor, at a nitrogen flow of 0.0171 g. moles sec.⁻¹ while triangular points represent data from the same reactor at 0.0125 g. moles sec.⁻¹. The square point represents data taken on the SOR reactor using average enthalpy determined at the slot. Also shown in this figure is a line segment representing the population of atomic nitrogen at 0.46 atmospheres as a function of enthalpy as calculated from equilibrium considerations (7). Two important conclusions can be drawn from this figure:

- d. The production of active species appears to be a smooth and reproducible function of enthalpy for a particular reactor regardless of flow rate.

- e. The population of active species correlates very poorly with nitrogen atom population based on average enthalpy, being many orders of magnitude too high at low enthalpy and a factor of 10 low at high enthalpy.

Pressure dependence. Although the experiment was principally run at a nominal reactor pressure of 350 torr some indication of sensitivity to pressure is necessary to assess the importance of the small pressure variations encountered. At a net power of 7000 ± 100 watts and a nitrogen flow of 0.0171 g. moles sec.^{-1} , the data of Table I were taken.

TABLE I

Relative Yield of HCN as a Function of Reactor
Pressure at Moderate Power

Total Reactor Pressure (torr)	195	350	484
n HCN/G	0.052	0.074	0.078
Heat Flow (watts)	6991	6992 (avg.)	7216
Conductance (mhos.)	1.27	0.58	0.68

Note that at 195 torr an appreciable fraction of the total enthalpy is tied up in directed kinetic energy so the free stream enthalpy is substantially lower than the heat flow would indicate. This leads to the further rather surprising observation:

- f. The fraction of nitrogen capable of ultimate reaction with the carbon containing species to HCN is nearly independent of reactor pressure.

Methane Utilization. Four gas samples were taken for mass spectrometric analysis at the 7000 watt level, corresponding to four points on the center curve of Figure 3, two below saturation and two above. Unreacted methane accounts for 10% of the methane flow at the highest flow rate ($\text{CH}_4/\text{H}_2 \approx 0.6$) but at all lower flows the conversion was found to be complete. In every case acetylene was found to be by far the major product, although for the points above the saturation value some carbon (a few percent) is found as other C_2 , C_4 and C_6 unsaturated hydrocarbons. If HCN production is estimated from Figure 3, the observed carbon balance is satisfactory to within the limited precision of the mass spectrometric analysis. This leads to the final observation:

- g. When the nitrogen is in excess all of the methane reacts to make for each molecule of HCN one of acetylene. When the methane is in excess, the excess methane that reacts forms chiefly acetylene, with minor amounts of C_4 and C_6 species.

DISCUSSION

General

In light of the observations a. and b. above, there would appear to be little question that the earlier interpretation (7) of the data taken on the SOR reactor was correct to the extent that a nitrogen plasma jet evidently contains some active species,

perhaps more than one, capable of reacting with the immediate decomposition products of methane to make HCN or its precursor. It seems equally clear that the procedure employed here quantitatively determines the flow rate of this (these) species.

Reactive Nitrogen Species

Atomic Nitrogen. From the welter of confusing evidence, and conflicting views that have accumulated over the decades of "active nitrogen" research, a sort of general agreement has recently been reached that at least the most important constituent must be atomic nitrogen in its ground state (1). With the high temperature thermal plasma investigated here it would seem that this possibility can be immediately excluded by observation. Taking into account all the known characteristics of a plasma-jet reactor, one can not account for the very low production rate of active species at high enthalpy. That is, on account of the intrinsic steep temperature gradient near the walls of a contained plasma-jet, one must always consider the possibility that the non-uniform radial temperature profile might cause observed effects. Furthermore, the enthalpy fluctuations to which a plasma jet is subject (9)

(9) M. P. Freeman, S. U. Li and W. vonJaskowsky, J. App. Phys. 33, 2845 (1962).

are not to be ignored. However, by actual computation one may very quickly satisfy himself that while a non-uniform temperature distribution might account for a total nitrogen atom population somewhat in excess of the average concentration calculated, no reasonable distribution of enthalpies could account for the observed dearth at high enthalpy.

Ionic Nitrogen. One of the theories of active nitrogen that has in the past enjoyed some popularity is that of Mitra (1). This theory invokes the molecular ion N_2^+ as the active species. This suggests attempting to correlate the production of active species with the rate of production of positive ions in the arc process. (The equilibrium population of ions at reactor conditions is much too small to be interesting.) This is, of course, just the rate of production of electrons, since the plasma remains electrically neutral. Note that at the higher power levels, even allowing for the considerable amount of heat involved in non-equilibrium ionization this implies, the temperature should still be high enough that the principal positively charged species is the atomic ion rather than the molecular ion. Since there is no reason to suppose that their ultimate products should be any different, this presents no difficulty.

A number proportional to the rate of production of electrons, and hence of positive ions, may be estimated in the following way: The conductivity, σ , in the actual arc discharge path is proportional to the density of electrons, n_e , and their mean free path (10). On allowing for the pressure dependence of the mean free path:

(10) H. O. G. Alfven, Cosmical Electrodynamics (Oxford, Clarendon Press, 1950) p. 47.

$$\sigma \propto n_e/P \quad [2]$$

There is also a weak temperature dependence, but this may be ignored as the temperature in the actual discharge path probably does not change much. If the discharge path occupies a fractional area, γ , of the total plasma-jet channel then the conductance M is proportional to:

$$M \propto \sigma \gamma \quad [3]$$

Now we make the assumption that the ion production rate, R , is just equal to the ion (and hence electron) population density in the discharge path times the velocity (proportional to $1/P$) of that part, γG , of the total flow, G , that flows through the discharge column:

$$R \propto n_e \gamma G/P \quad [4]$$

Combining [2], [3] and [4] we obtain the simple result that the conductance is proportional to the flow rate of ions out of the discharge path divided by the effluent flow rate:

$$M \propto R/G \quad [5]$$

Assuming that the heat flow, W , leaving the head is proportional to the energy actually dissipated in the arc (as opposed to energy dissipated to the cooling water in electrode processes) then from Watt's law:

$$R/G \propto I^2/W = M \text{ (mhos)} \quad [6]$$

Where I is the measured current through the head.

Figure 6 is a plot of conductance vs. relative rate of HCN production for all the data taken at 350 torr. Considering the crudeness of the derivation of [6] the agreement would seem to be extraordinarily good. It is fortunate that the analysis turns out to show little dependence on the reactor pressure as this variable was not held precisely constant for all the runs. Furthermore, this would seem to be consistent with observation elsewhere, despite the widely disparate reactor pressures employed, the active species production in the derivation of [6] now become apparent when one considers the conductance for it changes appreciably for the low pressure run. The points from the data of Table I are represented by asterisks on Figure 6. One might suppose the obvious disparity to be due to the arc length or mode of operation changing at low reactor pressure. As explained above, much larger changes in pressure are produced in the arc chamber by changing the flow rate than by changing the reactor pressure. Yet, if there is any real discrepancy between data taken at 0.0125 (Δ) and 0.0171 g. moles sec.⁻¹ (o) it is small.

Equilibrium Considerations. Apparently a charged specie (s) that persists in the jet is responsible for the observed HCN production rate. But now the question arises as to whether that species is present because of a slow recombination reaction and, hence large departures from local thermodynamic equilibrium (LTE) or whether it is due to the radial temperature profile discussed above. The square point in Figure 6, the datum for the SOR reactor, contributes a very direct answer to this question. For this reactor the methane is added only after the jet has been fired into a plenum, choked and then expanded. In the process it has lost nearly half the enthalpy it had on leaving the head: and yet it still agrees well with the correlation between HCN production and head conductivity exhibited by the TR reactor. Since even the maximum radial temperature in this case is well below that at which ions could exist at equilibrium, one must conclude that the back reaction destroying charged species in the jet is very slow compared to jet residence times (on the order of milliseconds for this reactor).

Another question that should be considered is whether so much enthalpy is tied up in non-equilibrium ionization that, assuming all other degrees of freedom to be equilibrated, the resulting temperatures are too low to allow an appreciable amount of atomic nitrogen. This could account for the unexpected lack of HCN generated by this species. However, in the worst possible case, subtracting from the

total enthalpy the heat of formation of a nitrogen ion for each HCN molecule formed, one finds that in the runs at highest heat flow there is still sufficient enthalpy to provide as much as 35% atomic nitrogen. Clearly one must look elsewhere to explain the inactivity of this species.

Unresolved Questions. It remains to identify, if possible the actual ionic species involved in the reaction from among the four likely candidates:



These may be quickly reduced to three by the following reasoning. If one positive ion is the reactive species then they both must be reactive since no difference is observed in Figure 6 between data taken at high power and at low. They must, in fact, be indistinguishable as reagents in this reaction. As a matter of convenience we may denote them both by the low temperature species, the molecular ion. Because the atomic ion is always surrounded by atoms and chilling is very rapid in the mixing zone of the reactor, it may be that the molecular ion is in fact the actual reagent.

The negative species presents more of a difficulty. It is certain that if charged particles of one sign are involved in the chemistry, so must particles of the opposite for the product emerges electrically neutral. The likely species to be involved, the electron gas, has certain drawbacks. Foremost among the drawbacks, it is hard to accept the slow recombination rate between electrons and positive ions implied. This would furthermore represent a disappointing departure from conventional active nitrogen research for by the use of microwave techniques Benson (6) has shown the concentration of electrons to be orders of magnitude too small to be paired in one-to-one correspondence with the active species (although the long persistence of conductivity could indicate the electrons were in equilibrium with some other species).

It has, to be sure, been almost axiomatic for three decades that the negative nitrogen ion can not form because in its ground state it is unstable, or nearly unstable, with respect to dissociation to the atom. However, Boldt (11) has recently

(11) G. Boldt, Z. f. Physik 154 330 (1959).

shown through spectroscopic evidence that a metastable nitride ion forms and persists in appreciable concentration in an arc discharge that is not appreciably different from the plasma generating arc employed here so that this possibility may not be lightly disregarded. The transition of this metastable ion to the ground state is spin forbidden. Its ionization potential is 1.1 ev to an excited metastable atomic state that lies 2.38 ev above the ground atomic state.

There would seem to be no good way to determine within the context of the present experiment whether the positive or negative species is involved in the reaction in a path determining way. More important perhaps within the context of active nitrogen research is the manifest inactivity of atomic nitrogen ... even under conditions of heavy methane flow.

Reactive Carbon Species

As a completely unexpected by-product of this work. observations c and g would seem to give interesting confirmation to the work of Skell and Wescott (12).

(12) P. S. Skell and L. D. Wescott, J. Am. Chem. Soc. 85, 1023 (1963).

These investigators have identified the principle species in carbon vapor at low pressures as a dicarbene:



[8]

by the chemical identification of its addition products with olefins when they are sublimed together onto a cold surface.

Observation c., that only one carbon atom in three may react to make HCN when the nitrogenous reactive species is in excess, the other two going to acetylene, is quite reasonably explained if in the principle step a nitrogen kernel is attached to a dicarbene which then subsequently forms one HCN and C_2H_2 . Observation g. follows equally well by postulating that when the dicarbene is in excess it dimerizes and then forms mono-, di-, and tri-acetylene units on subsequent attack by atomic hydrogen; partial hydrogenation of the higher acetylenes by atomic or molecular hydrogen to make vinyl- and divinyl-acetylene then completes the reaction sequence.

SUMMARY

This experiment, simple in concept and interpretation, would appear to shed considerable light on the details of the reaction of methane with a nitrogen plasma-jet. Although there are still many details requiring further work, at the present time we can propose the following simple concept for the reaction sequence:

1. A part of the nitrogen as it passes through the arc head unit, passes through the arc column or discharge path. There it is completely dissociated and ionized to the extent required by the arc process.
2. As the fresh gas enters the discharge column, atoms, atomic ions, and electrons are swept out where they mix with the relatively cold gas that is bypassing the discharge column.
3. The mixture equilibrates in most degrees of freedom to some reproducible steady state consisting of a mixture of at least atoms, molecules, atomic and molecular ions and electrons.
4. Some process leading to equilibration of that degree of freedom of the mixture involving the existence of the active species is effectively "frozen" or nearly so; the flow of active species in the stream is equal, or almost equal to the rate at which it or its precursor is displaced from the arc zone.
5. The rate at which the active species or its precursor is blown out of the arc zone is proportional to the rate at which charged particles of either sign are blown out, which is presumed to indicate that the active species or its precursor is charged.
6. As the end products are necessarily electrically neutral, ions of both polarities are required in the chemistry. Those with positive charge are probably an equilibrium mixture of the molecular and atomic ions, presumed to be chemically indistinguishable, while the negative charge carrier could be electrons, free nitride ion gas, or possibly some equilibrium mixture. From the present experiment there is no indication of the sign of the ions which initiate and determine the path of the reaction.
7. As the methane enters the reactor it rapidly mixes into the hot plasma and is converted to C_3 dicarbene molecules. The nitrogen containing active species

reacts with it to form one molecule of HCN and one of C_2H_2 on subsequent cooling and attack by atomic hydrogen. When the C_3 is in excess, the excess dimerizes; on subsequent cooling and attack by atomic hydrogen it goes mainly to acetylene with small amounts of C_4 and C_6 molecules with varying degrees of unsaturation.

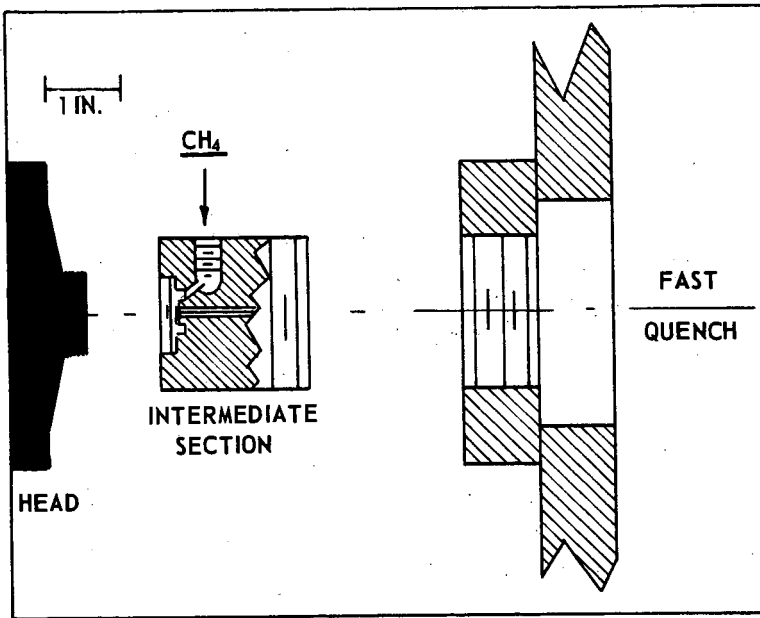
This reaction sequence is of course only appropriate to the plasma jet situation; however, the outstanding factor emerging from this study that one should keep in mind when considering the greater relevance of this work is that an active species has been found that has chemical properties generally attributed to ground state atomic nitrogen in conventional active nitrogen research. This species has been shown to be:

- a) Not atomic nitrogen in the ground state.
- b) In direct proportion to the number of charged particles produced in the arc process.

ACKNOWLEDGEMENT

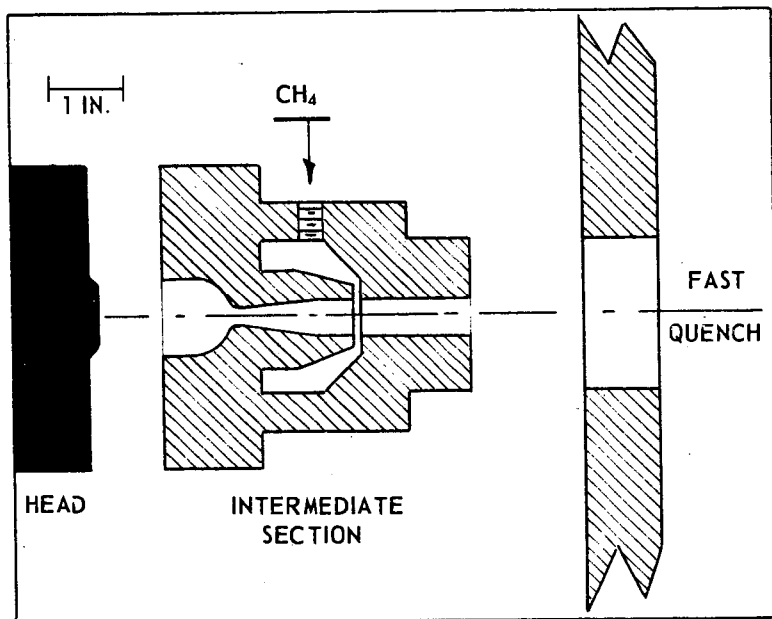
Among the numerous people who have contributed in some way to the conception and performance of the research the author must especially acknowledge the encouragement and helpful discussions of Drs. A. K. Hoffmann, H. M. Hulburt, J. E. Longfield and J. F. Skrivan, all of this organization. He wishes furthermore to acknowledge the considerable technical assistance of Mr. C. W. Beville.

Figure 1



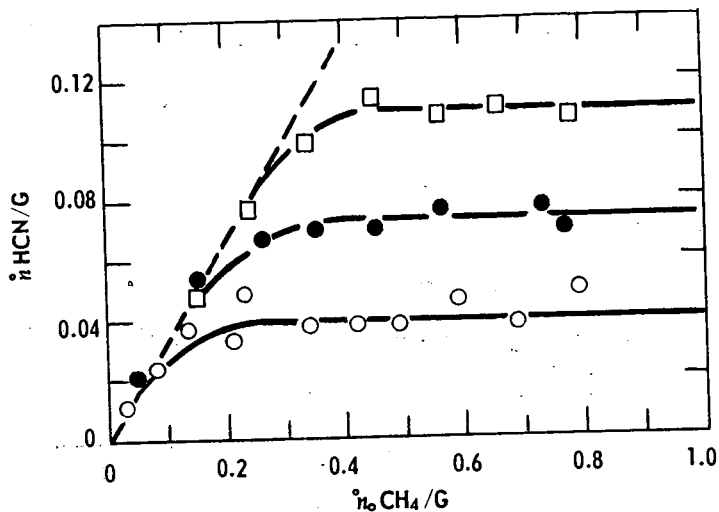
Exploded view of TR reactor. Intermediate section shown in simplified cross section. Material: Copper

Figure 2



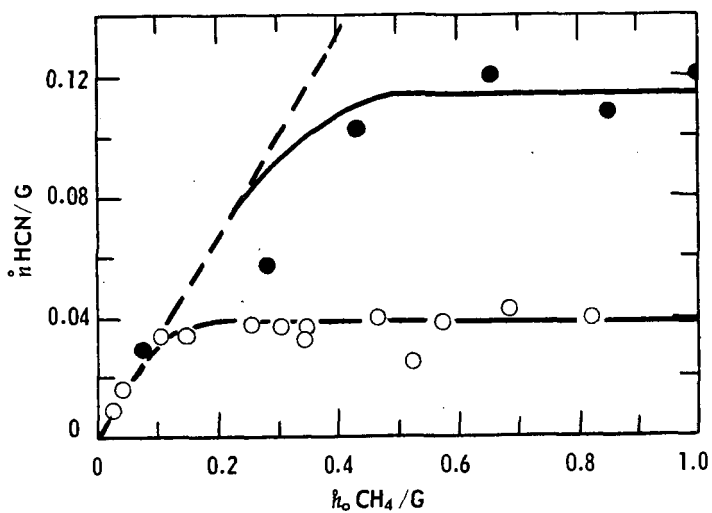
Exploded view of SOR reactor.
Intermediate section shown in simplified cross section.
Material: Copper

Figure 3



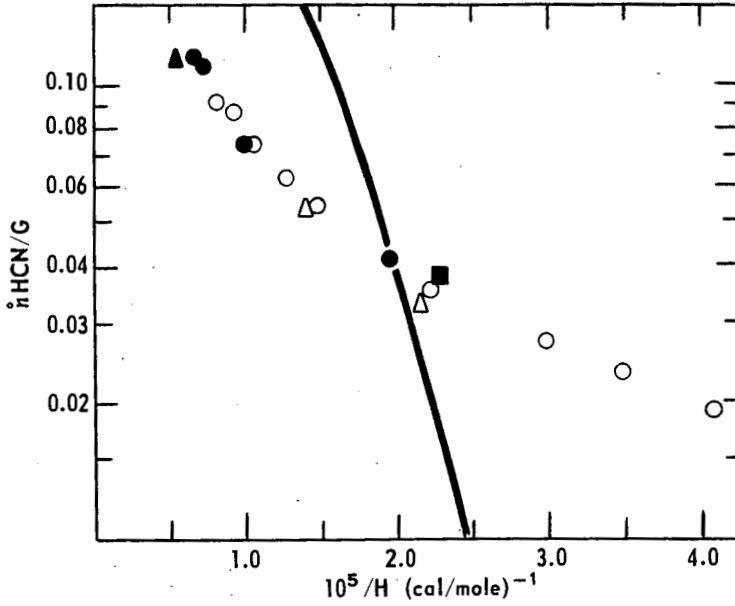
Rate of production of HCN vs. feed rate of methane (both relative to effluent nitrogen flow, G, of 0.0171 gram moles sec. $^{-1}$) at three net power levels: 3522 watts - \circ ; 6992 watts - \bullet ; and 9782 watts - \square TR reactor. Dashed line has slope of one-third.

Figure 4



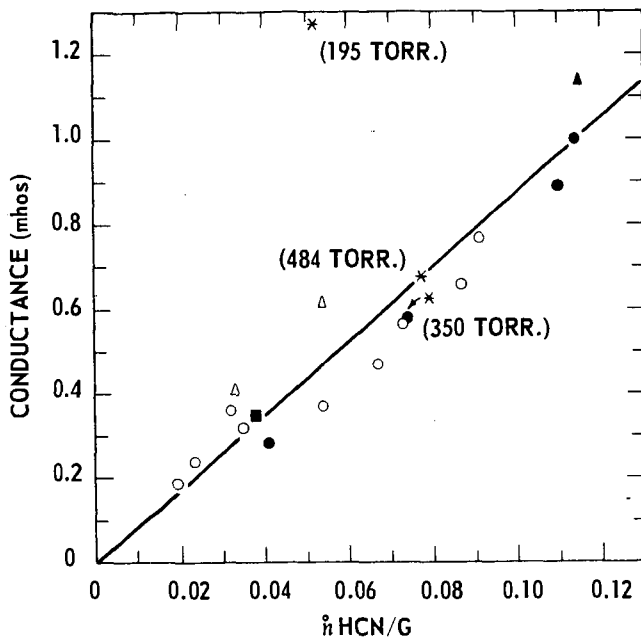
Same plot as Figure 3. ●-TR reactor at 9506 watts net power with reduced nitrogen flow ($G = 0.0125$ gram moles sec.^{-1}); highest enthalpy run. ○-SOR reactor at 2989 watts net power at feed slot ... power leaving head in gas was 5517 watts ... nitrogen feed rate 0.171 gram moles sec.^{-1} . Dashed line of slope one-third again shown.

Figure 5



Logarithmic plot of the flow rate of HCN (assumed equal to the flow rate of active species) relative to the flow rate of effluent nitrogen as a function of reciprocal average enthalpy at the point of introduction of methane. Point legend given in text. Line shown represents expected nitrogen atom population based on average enthalpy as calculated from equilibrium considerations.

Figure 6



Conductance (proportional to the fraction of nitrogen molecules ionized) vs. active species flow rate relative to effluent nitrogen. Legend of points corresponds to that of Figure 5. Points marked with asterisks correspond to the data of Table I.

HYDROCARBON REACTION IN CORONA DISCHARGE¹

M. Kawahata, J.C. Fraser, and J.A. Coffman

Advanced Technology Laboratories
General Electric Company
Schenectady, New York

-
1. This paper includes part of an investigation on "the coal hydrogenation by electric corona discharge", under the contract with the Office of Coal Research, Department of Interior.
-

INTRODUCTION

When an electric field (a-c in this paper) is applied to the series combination of a gaseous gap and a dielectric solid, the gas will break down and conduct at an applied voltage much lower than that required to break down the solid. The current increases rapidly with an increase in voltage. The dielectric barrier acts as a series ballast to stabilize the corona discharge, which appears as a "soft" glow electrical discharge. THIS FORM OF GLOW DISCHARGE AT ATMOSPHERIC PRESSURE IS DEFINED AS "CORONA"² in this paper. The dominant mechanism in corona

-
2. As contrasted with corona, the spark is a form of unstable discharge. Intense ionization along a definite path for a greater part of the electrode distance is a characteristic of spark. The arc is a form of concentrated spark characterized by a high current density at a relatively low voltage.
-

is ionization by electron impact. The free electrons in the gas acquire energy from the applied field, and, colliding with the gas molecules, create additional free electrons and positively charged ions.

Under stable corona electrical discharge in an electric field containing solid dielectric barriers, chemical reactions which only proceed with difficulty by conventional means may take place with reasonable efficiency. The chemical reactions caused by electric discharge are essentially those involving active species, like excited molecules, free radicals and ions, formed by inelastic collisions between accelerated electrons and molecules.

Extensive studies on the chemical reactions of aliphatic hydrocarbons under the electrical discharge were conducted in 1930's by Lind et al (3,4,5). Using methane as a reactant, the

-
3. S.C. Lind and G. Glockler, *J. Am. Chem. Soc.*, 51, 2811 (1931).
4. S.C. Lind and G.R. Schultze, *ibid.*, 53, 3355 (1931).
5. S.C. Lind and G.R. Schultze, *Trans. Electrochem. Soc.*, 59, 165 (1931).
-

formation of free radicals followed by production of molecular hydrogen, and also condensation to higher paraffins was the essential process. Also, the reaction scheme and the reaction products of α -radiolysis were studied. A similarity between reactions in the electric discharge and radiolysis, was postulated by Lind et al (6,7).

-
6. S.C. Lind and G. Glockler, J. Am. Chem. Soc., 52, 4450 (1930).
 7. S.C. Lind and D.C. Bardwell, J. Am. Chem. Soc., 48, 2335 (1926).
-

The radiolysis of methane was investigated more recently in detail, especially to clarify the reaction mechanisms, including the primary and the secondary reaction processes (8,9,10,11,12,13).

-
8. F.W. Lampe, J. Am. Chem. Soc., 79, 1055 (1957).
 9. K. Yang and P.J. Manno, J. Am. Chem. Soc., 81, 3507 (1959).
 10. G.G. Meisels, W.H. Hamill and R.R. Williams, J. Phys. Chem., 60, 790 (1956).
 11. G.G. Meisels, W.H. Hamill and R.R. Williams, J. Phys. Chem., 61, 1456 (1957).
 12. G.J. Mains and A.S. Newton, J. Phys. Chem. 64, 511 (1960).
 13. R.R. Williams, Jr., J. Phys. Chem. 66, 372 (1962).
-

High energy electrons, low energy electrons, γ -ray and x-ray irradiations were employed for decomposition of methane, producing mainly H_2 , C_2H_6 , C_3H_8 , C_4H_{10} , and C_5H_{12} . It was found that the energy yield of the reactions were essentially independent of the radiation source, dosage, and the system pressure (6,7,8,9,10,11,12,13,14). However, because of the extreme complexity of the reaction processes, the mechanism is not yet completely understood.

-
14. S. Shida, Hoshasen Kagaku (Radiation Chemistry), Nikkan-Kogyosha, Tokyo, Japan (1960).
-

Electrical discharge chemistry has not yet studied intensively from the standpoint of chemical engineering except for a few processes (15,16,17). In order to achieve the technical progress in this field,

-
15. T. Rummel, Hochspannungs Entladungsschemie und Ihre Industrielle Anwendung, Munchen, Germany (1951).
 16. G. Glockler, and S.C. Lind, The Electrochemistry of Gases and Other Dielectrics, New York (1939).
 17. Electric Engineering Soc. Ozonizer Committee, Japan, edited by Suzuki Corona-sha, Tokyo, Japan (1960).
-

according to Suzuki et al, it is highly important to investigate the correlation between electric discharge phenomena and the chemical reactions caused by discharge. This includes: (1) clarification of the concentration and energy distribution of ions and electrons in the discharge space, (2) understanding of the probability of excitation and dissociation caused by collisions of molecules with slow electrons, and (3) clarification of the complete energy balance in the discharge reaction.

Recently in this laboratory, studies on hydrocracking of coal, tar, and related hydrocarbons, using an electric discharge system have been undertaken. This work was primarily intended to obtain chemical engineering knowledge of electric discharge chemical processes. As part of the program, decomposition of methane was studied, since this gas is likely to be used as one of the reactants for cracking of hydrocarbons, and further its simple chemical structure is well suited to definitive studies. Similar studies using aliphatic hydrocarbons other than methane were also conducted but they will be reported elsewhere.

EXPERIMENTAL

Apparatus The experimental apparatus is shown schematically in Figure 1-a. Methane was fed to the reactor with a definite flow rate determined by a rotameter. Then, the product gases were passed through a sampling bottle and a dry testmeter. The reactors employed in this investigation were essentially concentric electric discharge tube similar to ozonizers. The dimensions and the materials of the electrodes were varied, as summarized in Table 1. In Table 1, the discharge space, V , in cc., total surface area, S , in cm^2 , and the logarithmic average of the outside and inside electrode area, A , in cm^2 are listed together. On one side of the quartz electrode, a silver or tin oxide coating served as the electrically conductive surface. In order to determine the reactor temperature, thermistors were attached to the outside electrode and a thermometer was placed in the inside electrode. The electrical system is shown schematically in Figure 1-b.

The corona generating equipment used in these experiments consists of a high voltage, high frequency power supply, with associated instrumentation to control and measure the corona power generated. The output of a 10,000 cycle, 30 KW, inductor-alternator is fed to the primary of a 50 KV, high voltage transformer and, in turn, to a tuned circuit, to a corona cell, and to the high voltage instrumentation. The Basic Power and Instrumentation Circuit is shown on Figure 1-b.

Inductor-alternator output voltage and subsequently, transformer high voltage, are controlled from zero to maximum output by varying the alternator field current.

Since the corona cell itself represents a capacitive load on the inductor-alternator and the transformer, a tuning circuit is provided for power factor correction, so that the high voltage transformer sees only the resistive load represented by the corona power dissipated in the corona cell. This tuning circuit consists of an air-core, foil wound choke and a vacuum-capacitor bank, connected as a parallel resonant circuit across the transformer secondary.

High voltage instrumentation includes a vacuum tube voltmeter operating from a capacitance voltage divider, for reading the peak voltage applied to the corona cell, and a bridge circuit for determining corona power by means of the parallelogram-oscilloscope technique. This technique shows the relationship between the voltage on the cell electrodes at any instant and the charge flow in the circuit up to that instant. Using the area of parallelogram on the oscilloscope, the power input (18) to the reactor was computed.

-
18. The power dissipated in a concentric cylinder corona cell consisting of a gaseous gap in series with solid dielectric barriers can also be calculated from the expression:

$$P = 4fC_b V_g (V_m - V_t)$$

where P is power in watts,
 f is power supply frequency, c.p.s.,
 C_b is capacitance of the dielectric barriers,
 V_g is voltage across gaseous gap at the instant of corona initiation
 V_t is total voltage applied to the corona cell at the instant of corona initiation, and
 V_m is corona cell operating voltage, at some value greater than V_t .

In the above calculation, peak voltage values are used.

Procedures The entire system was first evacuated and methane was introduced to the reactor with a definite flow rate. The voltage applied to the reactor was gradually increased to the gas-space breakdown voltage, at which the electric discharge was initiated. Then, the voltage was adjusted until the parallelogram on the oscilloscope showed the desired discharge wattage. The discharge power was maintained constant during the run. The reaction was usually continued at least for 30 minutes before samples were taken. If there was liquid product in the condenser-I, it was weighed but no attempt was made to analyze it. The gaseous samples were analyzed by mass spectrometer. For reaction at higher temperatures, the methane was heated to the desired temperature in a preheater which was equipped with a temperature controller (West Co.).

EXPERIMENTAL RESULTS

Variation of the Composition with Residence Time The principal reaction products were hydrogen, ethane, propane, butane, pentane and further higher paraffins. In some experimental runs, a small amount of ethylene and propylene was found. In Figure 2 and 3, the variation of the composition with residence time is shown. These two sets of runs were conducted at temperatures between 200 and 230°C under a pressure of 760 mm Hg. The model III reactor was employed, and the current density levels were 0.13 and 0.15 ma./cm.². The current density was computed by using the voltage in the discharge space calculated from the total voltage applied, the discharge wattage and the logarithmic average area of the electrodes A, listed in Table 1. In these figures, the fraction C_2 and C_3 include ethylene and propylene, respectively, and the fraction $+C_4$ includes all the higher paraffin homologues.

It was observed that the disappearance of methane and the formation of H_2 , C_2 , C_3 and $+C_4$ were more rapid at the higher current density. In the initial period methane was consumed almost proportionally to time. This fact agrees to the results reported by Lind and Schultze(3) After this period, methane disappeared exponentially with time. It must be noted that in each of three runs having residence time longer than 100 seconds produced a small amount of liquid which was of amber color.

Effect of Temperature on the Initial Rate of Reaction Using the Model II and IV-C reactor, the initial rate of methane disappearance was investigated varying the reaction temperature. The reaction temperature was determined by taking the average of the inside and outside electrode temperatures. In Figure 4, is shown the Arrhenius plot of the initial rate of CH_4 disappearance in atm./sec. Two lines, AA and

BB, could be drawn, and the apparent activation energy of the overall reaction was calculated to be 4 Kcal./mol. The points along the line AA were determined at a current density of 0.095 ma./cm.² and an applied potential of 5 to 5.2 KV. across the discharge space using the model III reactor. The points along the line BB were determined at a current density of 0.15 to 0.17 ma./cm.² using the model IV-C reactor at 4.5 to 5.0 KV. across the discharge space. Both series were made under a pressure of one atmosphere.

Effect of Current Density on the Initial Rate of Reaction In order to correlate the initial rate of methane disappearance with current density, the rate of reaction at 200°C was computed from each rate obtained at various reaction temperatures by using the activation energy of 4 Kcal./mol. (The temperature, 200°C, is just an arbitrary temperature.) The computed rates of reaction are plotted against current density in Figure 5. The rate of reaction increased as the current density increased, following a relationship,

$$-\frac{d(\text{CH}_4)}{dt} = k(j) \quad (1)$$

where the rate is in atm./sec., the current density, j , is in ma./cm.², and k is 0.075 in average.

Electric Discharge in Space Packed with Alundum Grains and Effect of Pressure on the Rate of Reaction The discharge space of the model IV-B reactor was packed with alundum grains having a particle size of 10 x 15 Tyler mesh, to determine any consequent effect on the reaction rate. The total pressure of the system was also varied in two experimental runs. The experimental results are summarized in Table II. For this packed space reactor, the applied voltage required to initiate the discharge was greater and the discharge wattage was smaller than for the reactor without packing. For the packed discharge space reactor, the apparent current density and the apparent reaction rate are listed in Table II. The apparent dielectric constant of the space packed with alundum grains was calculated using Kamiyoshi's correlation (19), and

-
19. K. Kamiyoshi, Science Reports, Res. Inst. Tohoku Univ. Ser.A, 1, 305 (1949), C.A. 45, 5991
-

then the voltage applied to the packed discharge space and the apparent current density were estimated. For better comparison, the reaction rate at 200°C. was calculated for each run and listed in Table II. Since the rate increases with power density, it is seen that the reaction rate is considerably higher in the packed space reactor, and lower at reduced pressure.

Effect of the Uniformity of the Field on the Reaction Rate Using the several reactors having different diameter ratio, D_i/d_o , (the ratio between the inside diameter of the outside-electrode and the outside diameter of the inside-electrode), the possible effect of non-uniformity of the field on the reaction rate was investigated. It must be noted that for the model IV-D and the IV-E reactor, the inside electrode was tungsten rod or wire. (This type of reactor was called a semi-corona reactor by Lind et al.) The catalytic effect of the tungsten surface was assumed insignificant. It was observed that for these two reactors, discharge streamers were formed only around the center electrode, whereas in the other model reactors, numerous fine blueish streamers extended

from the inside electrode to the outside electrode resulting in formation of blue glow in all the discharge space.

The experimental results are listed in Table III. In the second experimental run, the IV-D reactor failed by arcing between the electrodes. Similarly, the experiment using the IV-E reactor was hindered by the formation of several hot spots on the tungsten electrode which resulted in arc-over between the electrodes. For better comparison, the reaction rates at 200°C were calculated using an activation energy of 4 Kcal/mol. and they are also listed in Table III. Taking into account the difference in current density, the reaction rate seemed lower in the reactor having larger D_i/d_o .

DISCUSSIONS

Based on studies of the radiolysis of methane, the following four steps may be considered to be of primary importance in the decomposition of methane by electric discharge:

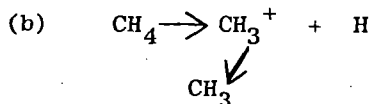
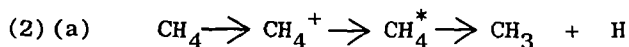
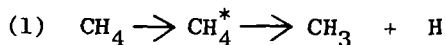
- (1) Formation of excited molecules by inelastic collisions with electrons having sufficiently high energy, and subsequent decomposition to free radicals and/or atoms.
- (2) Ionization of molecules and subsequent neutralization of ions, resulting in formation of free radicals.
- (3) Ion-molecule reactions (20), forming larger ions, and subsequent neutralization leading to formation of neutral molecules and free radicals.

20. F.W. Lampe, J.L. Franklin, and F.H. Field, Kinetics of the Reactions of Ions with Molecules, in Progress in Reaction Kinetics, Vol. I, 67, Pergamon Press, New York, (1961).

- (4) Combination of free radicals or reaction of free radicals with molecules (21).

21. E.W.R. Steacie, Atomic and Free Radical Reactions, Reinhold Publishing Corp., New York (1954).

Thus, for example, the formation of ethane could be explained by the following steps:



If more than one kind of electron-reactant reaction is involved simultaneously, integral must be replaced by the sum of the integrals. In this investigation, the initial rate of methane consumption was found to be proportional to the current density when other factors are kept constant. Except for the initial time period, proportionality of the rate to the partial pressure of the reactant was also found as shown in Figure 2 and 3 which show the variation of methane concentration exponential to time. Taking into account the difference in current density, it is seen that proportionality between the rate and the pressure somewhat deviates for the packed bed reactor shown in Table II. This may be due to an uncertainty in estimation of the apparent dielectric constant of the alundum grains packed space and, therefore, in current density. However, as a first approximation, equation (2) seems to apply to this work.

Before corona is initiated the total applied voltage is distributed across the cell components inversely as their capacitance. Then, the voltage and gradients in a concentric cylinder reactor, just before the start of corona, can be expressed by the following expression:

$$E = \frac{V}{r k_g} \left[\frac{1}{\ln \left[\frac{(D_o/D_i)(d_o/d_i)}{k_b} \right] + \frac{\ln(D_i/d_o)}{k_g}} \right] \quad (3)$$

where, E is the field at any point in radius, r ,
 V is the total applied voltage,
 k_g and k_b are the dielectric constant for gas and barrier,
 respectively,
 D_o and D_i are the outside and inside diameter of the outside
 electrode, and
 d_o and d_i are the outside and inside diameter of the inside
 electrode.

After corona is initiated, the total applied voltage is distributed across the cell components directly as their impedance. However, this does not alter the equation (3) greatly.

Since,

$$\left(\frac{D_o}{D_i} \right) \left(\frac{d_o}{d_i} \right) \sim 1.0, \quad (4)$$

the equation (3) becomes

$$E \sim \frac{(1)}{(r)} \left[\frac{V}{\ln(D_i/d_o)} \right] \quad (5)$$

The drift velocity, W , and the integral term in equation (2) are a function of E/p , where p is the pressure. Thus, the overall rate of reaction becomes the integral of the equation (2) with respect to radial distance. Increasing the diameter ratio, D_i/d_o , appeared to cause a decrease in the overall rate of reaction. Since the exact expressions of $Q(V)$, $f(V)$, and W are not available, the analysis of the data is qualitative. Nevertheless, for the reactor having larger D_i/d_o , apparently a possible faster reaction rate in the strong field near the center electrode was overbalanced by the slower rate in the weak field portion of the reactor.

The rate of reaction was significantly increased, when the reactor discharge space was packed with alundum grains. This increase in the

rate cannot be explained clearly. Higher field in the packed space, surface reaction effects, if any, or higher concentration of high energy electrons in a smoothly diffused discharge formed in a packed space could be the reasons.

The energy yield of the process is shown in Figure 6, where energy introduced per unit mol. is plotted against methane consumption in per cent. The calculated reaction rates at 200°C were used for the plot. The slope, that is, the average energy spent per mol. of methane consumed was 1980 Kcal/mol. at 200°C for the initial period. The best result was obtained for the alundum grain packed reactor at 267°C. and the energy yields were 740, 1090, 3000, and 9000 Kcal per mol. of CH₄ disappearance, and H₂, C₂H₆ and +C₃ formation, respectively. The corresponding G values were 3.1 (-CH₄), 2.1 (H₂), 0.77 (C₂H₆) and 0.26 (+C₃). These values are about one-half of the values obtained by radiolysis (6,7,8,9,10,11,12,13,14).

ACKNOWLEDGEMENTS

The authors wish to thank T. H. Phoenix and G.A. Techy for their assistance in this experimental work, G. P. Schacher for mass spectrographic analysis, and N. R. Dibelius and C. D. Doyle for valuable discussions.

TABLE I
DIMENSIONS OF THE REACTORS

Reactor	Outside Electrode			Material	Inside Electrode		
	O.D. D_o mm	I.D. D_i mm	Material		O.D. d_o mm	I.D. d_i mm	Material
II	19.0	17.0	quartz	11.0	9.0	quartz	
III	45.7	42.4	quartz	35.3	32.0	quartz	
IV-A	45.7	42.4	quartz	35.3	32.0	quartz	
IV-B	20.0	18.0	quartz	12.0	10.0	quartz	
IV-C	12.1	10.0	quartz	4.0	3.0	quartz	
IV-D	9.5	7.3	tungsten	1.05	---	tungsten	
IV-E	8.5	8.3	tungsten	0.33	---	tungsten	

Reactor	Electrode Length L mm.	Discharge Space V cc.	Total Area S cm. ²	Average Cylindrical Area A cm. ²	Diameter Ratio D_i/d_o
II	78	10.3	71.7	34.0	1.5
III	400	168.0	975.0	488.0	1.2
IV-A	200	84.0	488.0	244.0	1.2
IV-B	200	29.0	188.0	93.0	1.5
IV-C	200	13.2	87.5	41.0	2.5
IV-D	200	8.2	52.5	20.4	7.0
IV-E	200	6.2	41.5	12.7	19.0

TABLE II

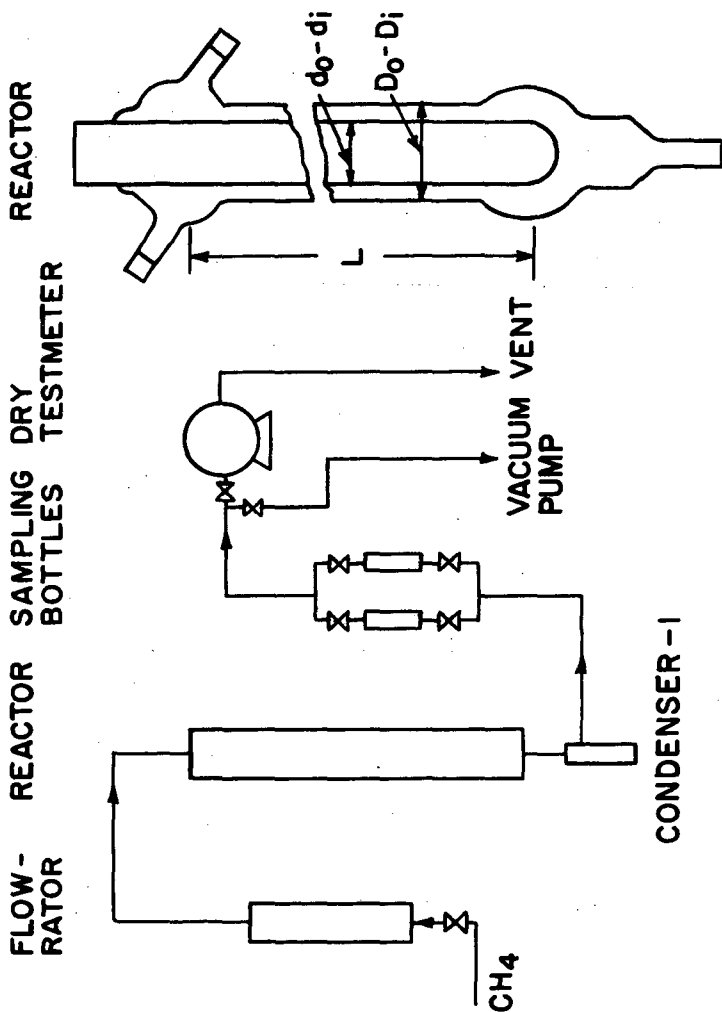
EFFECT OF THE REACTOR SPACE PACKED WITH ALUNDUM
GRAINS AND OF PRESSURES ON THE REACTION RATE
(IV-B REACTOR)

Exp. No.	Reactor Packing	Pressure mm.Hg	Temp. °C.	KV kv. g	Current Density, $2j$ ma./cm. ²	Rate (atm./sec.) $\times 10^2$	Computed Rate at 200°C (atm./sec.) $\times 10^2$
9-24-3-1	no	760	280	5.1	0.17	2.7	1.5
9-24-3-2	Al ₂ O ₃ grains	760	267	5.8	0.083	2.1	1.3
9-25-3-1	Al ₂ O ₃ grains	238	225	4.1	0.13	1.6	1.3
9-25-3-2	Al ₂ O ₃ grains	280	325	4.0	0.12	2.2	0.87

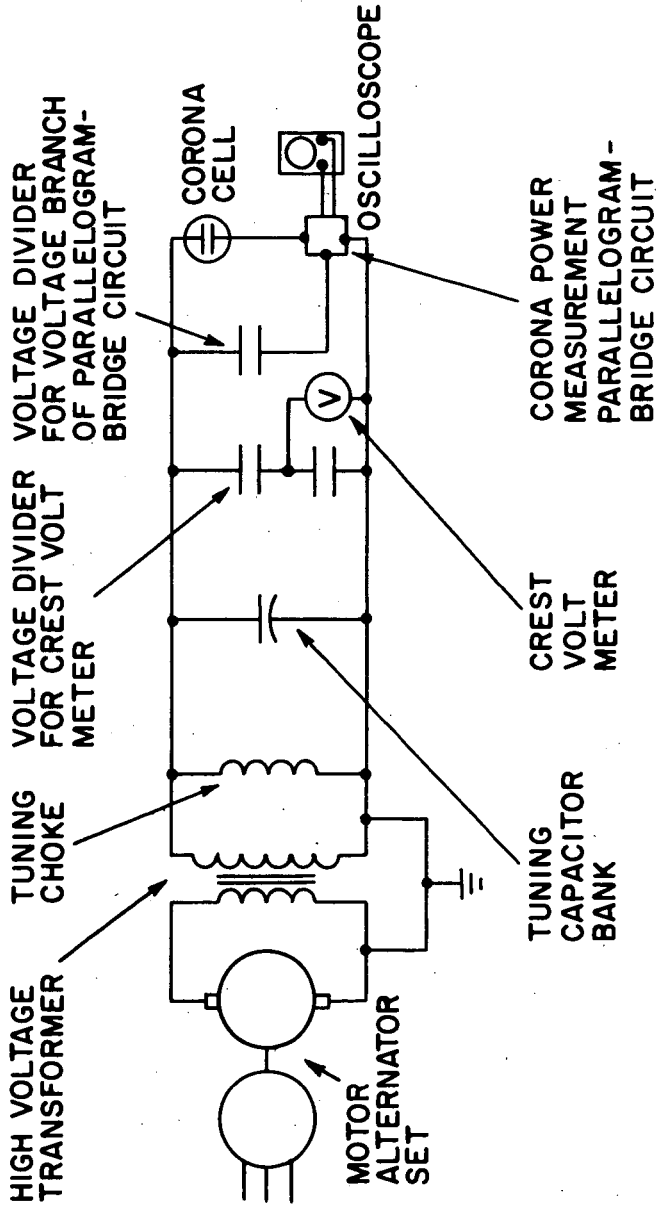
TABLE III

EFFECT OF UNIFORMITY OF THE FIELD ON THE REACTION RATE

Exp. No.	Reactor	D _i /d _o	Temp. °C.	KV kv. g	Current Density, $2j$ ma./cm. ²	Rate (atm./sec.) $\times 10^2$	Computed Rate at 200°C (atm./sec.) $\times 10^2$
9-24-3-1	IV-B	1.5	280	5.1	0.17	2.7	1.5
9-9-3	IV-C	2.5	215	5.0	0.15	1.1	1.0
9-11-31-1	IV-C	2.5	318	4.5	0.18	2.7	1.2
9-6-3	IV-D	7.0	217	4.8	0.32	1.9	1.7
9-16-3-1	IV-E	19.0	80	3.9	0.33	0.33	1.4
9-16-3-2	IV-E	19.0	110	4.4	0.32	0.48	1.3

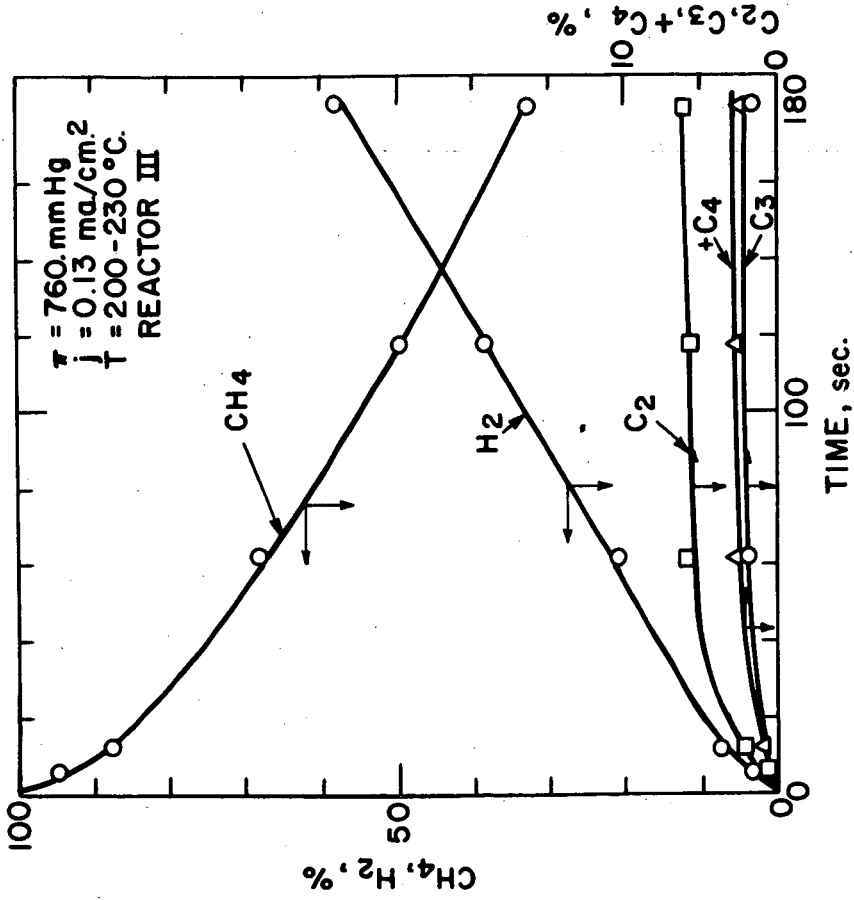


FLOW DIAGRAM OF THE APPARATUS
AND THE REACTOR
FIGURE 1-a

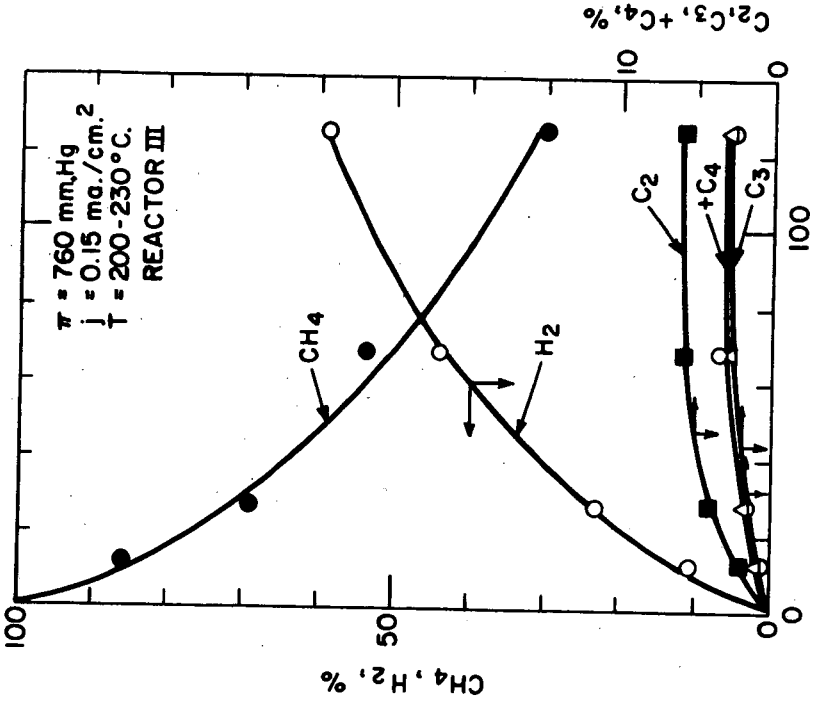


BASIC POWER AND INSTRUMENTATION CIRCUIT

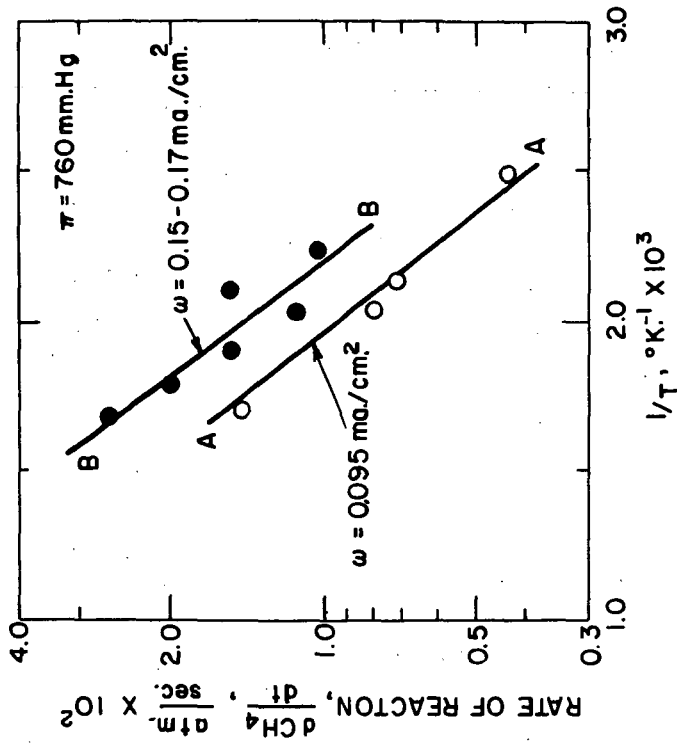
FIGURE 1-b



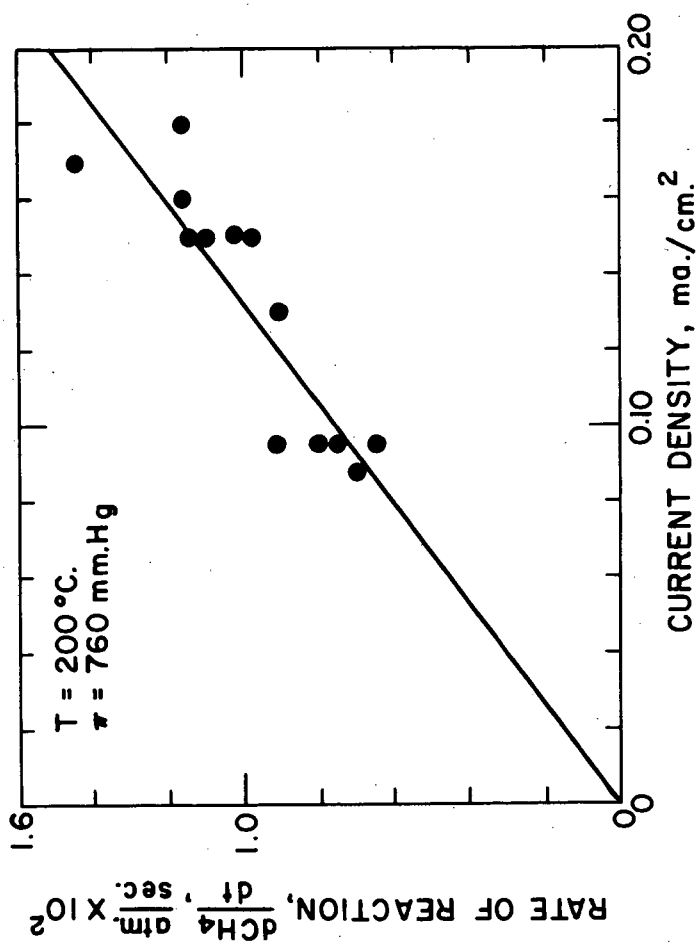
VARIATION OF COMPOSITION OF PRODUCT GASES WITH TIME
FIGURE 2



VARIATION OF COMPOSITION OF PRODUCT GASES WITH TIME
FIGURE 3

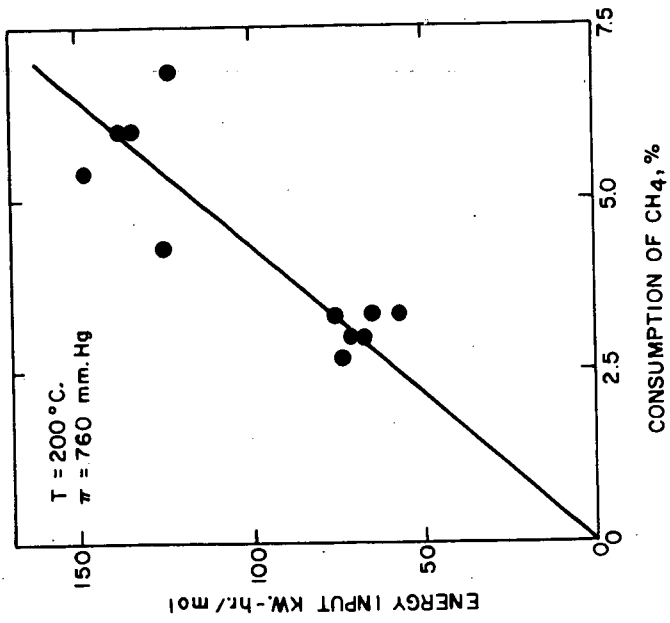


ARRHENIUS PLOT OF THE OVERALL
 RATE OF REACTION
 FIGURE 4



VARIATION OF RATE OF REACTION
WITH CURRENT DENSITY

FIGURE 5



VARIATION OF CH₄ CONSUMPTION
WITH ENERGY INPUT
FIGURE 6

PLASMA POLYMERIZATION

F. J. Vastola and B. Greco

Department of Fuel Technology, The Pennsylvania State University,
University Park, Pennsylvania

INTRODUCTION

Previous work with plasmas produced from hydrocarbons (1) demonstrated that both gaseous and solid plasma rearrangement products are produced. The distribution of these products depends upon the atomic hydrogen to carbon ratio of the reacting material. A limiting H/C ratio of approximately 1.6 was found for the solid. If the atomic H/C ratio of the starting material was greater than 1.6 both solid and gaseous products were formed, if the ratio was less than 1.6 only solid material was formed. With reacting gas ratios of less than 1.6 the solid would tend to have the same H/C ratio as the reacting gas.

The polymers produced by this process only depend upon the H/C ratio of the plasma and are independent of the molecular structure of the original reactants. With plasmas produced from single gases only a limited number of H/C ratios are available. However, by copolymerization of multicomponent mixtures solids of varying H/C ratio (max.=1.6) can be produced.

EXPERIMENTAL

Materials - Hydrogen (extra dry), acetylene (prepurified) and methane (CP) were obtained from the Matheson Co. The diacetylene was prepared according to the method described by Armitage, et al., (2) and purified by distillation.

Apparatus - The plasma generator consisted of a Raytheon* Diatherm unit (Model CMD 10) coupled to an Ophthos** cylindrical cavity. The frequency of the plasma generator was 2450 Mc. and the maximum output was 85 watts. The plasma reactions were carried out in a Pyrex bulb (vol.=150cc.) with a Vycor finger (OD=13mm).

Procedure - The experimental procedure consisted of filling the reaction bulbs with the reacting gas and analyzing the mixture mass spectrometrically before and after discharge; the H/C ratio of the solid produced is determined by making a material balance. The actual discharge takes place in the Vycor finger of the reaction bulb. The Vycor finger is positioned along the central axis of the cylindrical microwave cavity.

* Raytheon Co., Burlington, Mass.

** Ophthos Instrument Co., Rockville, Md.

RESULTS

Table I illustrates the relationship between the H/C ratio of the starting material and the H/C ratio of the solid produced.

Table I
DISCHARGE CHARACTERISTICS OF VARIOUS HYDROCARBONS

Mixture	H/C		Pressure, torr		Polymer Appearance
	Before Discharge	After Discharge	Before Discharge	After Discharge	
CH ₄	4.00	1.60	3.49	3.86	Clear
C ₄ H ₂ -H ₂	2.37	1.60	5.08	1.79	"
C ₂ H ₂ -H ₂	1.59	1.48	5.40	0.53	"
C ₂ H ₂ -H ₂	1.45	1.38	4.70	0.25	Very light brown
C ₄ H ₂ -CH ₄	1.38	1.28	3.75	0.67	"
C ₄ H ₂ -CH ₄	1.31	1.26	2.50	0.10	Light brown
C ₄ H ₂ -H ₂	1.23	1.20	2.70	0.05	"
C ₂ H ₂ -H ₂	1.20	1.20	4.10	0.02	"
C ₄ H ₂ -H ₂	1.20	1.19	5.42	0.15	"
C ₂ H ₂	1.00	1.00	5.02	0.03	Brown
C ₂ H ₂	1.00	1.00	4.90	0.03	"
C ₄ H ₂ -CH ₄	0.80	0.80	4.85	0.08	Dark brown
C ₄ H ₂ -H ₂	0.80	0.80	5.32	0.02	"
C ₄ H ₂	0.50	0.50	2.72	0.06	Very dark brown
C ₄ H ₂	0.50	0.50	3.35	0.02	"

If the initial H/C ratio is greater than 1.6 the solid will have a limiting H/C ratio of 1.6 and the remainder of the hydrogen and carbon in the system will be in the gas phase. Table II gives the composition of the gases remaining after a discharge lasting 120 seconds for a plasma produced from methane (H/C=4) and one produced from a diacetylene-hydrogen mixture (H/C=2.37).

Table II
Analysis, mole %

	CH ₄		C ₄ H ₂ -H ₂	
	Before Discharge	After Discharge	Before Discharge	After Discharge
H ₂	---	49	79	89
CH ₄	100	50	--	3
C ₂ H ₂	---	1	--	--
C ₄ H ₂	---	--	21	8

With a H/C ratio of less than 1.6 most of the starting material will be incorporated in the solid, and the discharge will be extinguished when the pressure remaining in the reactor reaches the lower pressure limit of the plasma generator.

Table III gives the time elapsed before a discharge will be extinguished for a series of diacetylene-hydrogen mixtures of constant total pressure and varying H/C ratio.

Table III
Plasma Extinction Time for $C_2H_4-H_2$ Mixtures

Total Pressure, torr	Ratio	Discharge Time, sec.
2.0	1.22	15
2.0	1.41	22
2.0	1.53	31
2.0	1.66	> 120

DISCUSSION

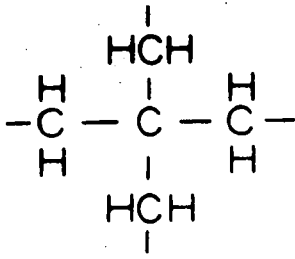
A hydrocarbon solid is one of the stable products formed by a hydrogen-carbon plasma. The maximum H/C ratio of this solid is approximately 1.6. This value cannot be exceeded even in cases where the H/C ratio of the plasma is greater than 1.6. The minimum H/C ratio of the solid is determined by the minimum H/C ratio of the hydrocarbon that is used for the plasma discharge, in this work the minimum H/C was 0.5 (diacetylene, C_4H_2). Table III illustrates that it is more difficult to produce solids as the H/C ratio approaches 1.6.

The physical appearance of the solids varied in a continuous manner from a clear, flexible film of H/C=1.6 to a very dark brown, brittle film of H/C=0.5. Infrared absorption analysis indicated no measureable aromatic structure even with a H/C ratio of 0.5. Absorption in the wave length regions 6.2 and 3.0-3.15 microns increased as the H/C ratio approached 0.5 indicating an increase in the degree of unsaturation. The decomposition products resulting from vacuum pyrolysis of the polymers were primarily hydrogen with a lesser amount of hydrocarbon gases ranging up to C_{10} . The majority of the C_4 to C_{10} hydrocarbons were highly branched compounds. No solvent was found for any of the polymers.

A possible structure for an insoluble, saturated aliphatic polymer with a H/C ratio of 1.6 is shown in Figure 1(a). This tetrahedral monomeric unit would form a three dimensional highly branched polymer; further hydrogenation would tend to destroy the polymeric structure. Since the polymers produced with H/C ratios varying from 0.5 to 1.6 seem to be part of a series, the structures shown in Figure 1(b) and 1(c) are possibilities of varying degrees of saturation of the basic monomer unit.

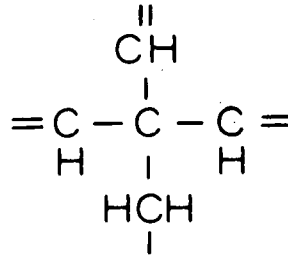
REFERENCES

1. F. J. Vastola and J. P. Wightman, *J. Appl. Chem.*, in press.
2. J. B. Armitage, E. R. H. Jones, and N. C. Whiting, *J. Chem. Soc.*, (1951), 44.



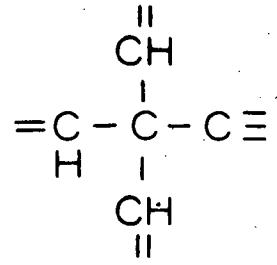
$$\text{H/C} = 1.6$$

(a)



$$\text{H/C} = 1.0$$

(b)



$$\text{H/C} = 0.6$$

(c)

MONOMER STRUCTURE FOR VARIOUS H/C RATIOS

FIGURE 1

Activation of Plastic Surfaces in a Plasmajet

Russell M. Mantell and William L. Ormand

AeroChem Research Laboratories, Inc.
Princeton, New Jersey

INTRODUCTION

The surface of a polymer such as polyethylene is difficult to paint, print, dye or laminate, unless previously prepared.¹ Methods of activating polymer surfaces may be conveniently divided into chemical, thermal, corona discharge, and the described non-equilibrium plasmajet types.

Typical chemical methods employ chromic acid solutions² or a combination of ozone and hydrogen halide.³ They do not appear to be of commercial importance.

Thermal methods which have been utilized industrially impinge heated air upon the surface⁴ while cooling the bulk of the plastic. The air is either preheated⁴ or a direct flame⁵ may be played on the surface.

Corona discharge methods, of recent industrial importance, pass polyethylene film over a rotating drum electrode while discharging a high frequency alternating current to the drum through a small air gap from a knife-edge electrode.⁶ Disadvantages of this process include puncturing of the polymer, inapplicability to inert, polar or readily-degraded polymers, and difficulties encountered in the treatment of irregularly-shaped or partly-conducting objects.

All of the above methods appear to involve some form of oxidation of the surface polymer while minimizing degradation of the bulk polymer. It is a convenient oversimplification to assume the thermal methods utilize diatomic oxygen, the corona discharge methods utilize triatomic oxygen, and a nonequilibrium

plasmajet method would utilize monoatomic oxygen. The latter was presumed to be the most reactive of the three oxygen species at low temperatures. Therefore, the oxygen plasmajet process was investigated in the hope of obtaining a novel,⁸ rapid and economical process for surface treatment capable of application to a variety of polymer surfaces.

The proposed plasmajet process described below utilizes a stream of oxygen which is partially dissociated by a glow discharge, expanded at high velocity through an orifice into a region of lower pressure, and then impinged upon the surface.

EXPERIMENTAL

Apparatus. The nonequilibrium plasmajet equipment utilized for the research is described elsewhere.^{9,10} It was modified by insertion, 12 inches downstream from the nozzle electrode, of a quick-opening Pyrex port of 4 inch I.D. by 12 inch length (measured at 90° from the axial reactor center). The port was closed by a 3/4 inch thick "Lucite" sheet, centrally drilled and tapped for a brass sleeve through which was loosely fitted a 1/4 inch diameter metal rod terminating in a 3 inch diameter by 1/4 inch thick brass target. The target was mounted so that the gas flow was parallel to the sample surface. Covering the target was a detachable metal hood into which the target and sample fit snugly to prevent exposure while operating conditions were being established. A thin Teflon sheet, cemented within the hood, contacted the plastic surface to be treated, to minimize abrasion. The hood and target arrangement was such that the specimen could be exposed at any desired distance from the jet axis. Vacuum-tight sliding seals were obtained by means of lubricated rubber couplings. The port permitted removal of the target and specimen within seconds after specimen exposure to permit an estimation by the use of a surface thermocouple of the film temperature attained. Insertion of the port into the apparatus was possible at various distances downstream from the nozzle electrode. Provisions were made for operation of the apparatus in a darkened room in order to permit visual observation of afterglow phenomena.

Materials. Oxygen, extra dry grade, and helium, 99.99% purity, were obtained in cylinders from the Matheson Company and dried immediately before entrance into the reactor by passage over activated alumina.

The following polymer samples were supplied through the kindness of the manufacturers: polypropylene, pro-fax type 6420 (Hercules); polyethylene, hi-fax type 1625 (Hercules); polyester, Mylar (duPont); polytetrafluoroethylene, Teflon type T.F.E. (duPont); polytrifluorochloroethylene, Kel-F type KX 8202 (3M Corp.); and polyvinyl fluoride, Tedlar type 50-SG20 TR (duPont).

The printing ink, Excellobrite White 500 (Sun Chemical Corp.) was similarly obtained. The lacquer employed was Duragloss, Camelia (A. R. Winarick, Inc.); the India Ink used was Pelikan Waterproof Drawing Ink (Gunther Wagner Co.) and the pressure-sensitive resin was "Scotch" Brand 600 acetate tape (3M Corp.)

Weightings. To remove electrostatic charges, a sample of the desired film, 1.0 mil thickness by 3.0 inches in diameter, was placed on the target, hooded and subjected to a 200 to 300 watt discharge at a pressure of about 1.0 Torr for a period of one second. The specimen was immediately weighed to 1/10 mg. on an analytical balance, replaced in the apparatus, exposed to the partially dissociated oxygen stream, reweighed and stored in air-tight containers. Finger cots and forceps were used in handling the specimens at all times.

Scratch Test. Exposed and control specimens of film were painted with commercial printing ink, lacquer and drawing ink, air-dried for at least 24 hours at room temperature, and manually scratched with a pointed stylus. Ratings were 1, 2 or 3 on a scale corresponding to unimproved, improved or greatly improved resistance to scratch removal relative to the control specimen.

Peel Strength Test. Exposed and control specimens of film were cut to 1/2 inch width and welded to pressure-sensitive tape of equal width. The weld was peeled apart at one end of the laminate. From the peeled end, the polymer was secured to a fixed point and the pressure-sensitive tape was attached to a balance pan, the weld itself being perpendicular to the force to be applied. The minimum force, in grams per inch, necessary to peel apart the remainder of the weld¹¹ was obtained by a successive increase of weights on the balance pan.

Surface Wetting Test. Exposed and control film specimens were secured to a horizontal table. A drop of water of 0.05 ml. volume was placed upon the film and the table slowly raised toward the vertical by a gear arrangement until the drop began to move across the surface. The angle which the film surface then made

with the horizontal is a measure of its surface wetting by water¹² and has been related to the adhesive properties of the film.¹³

Conditions. Unless otherwise noted, the conditions employed were as follows: 6 inch discharge electrode gap, 5/16 inch nozzle orifice diameter, 1 mil by 3 inch diameter sample, downstream pressure 3 Torr, upstream pressure 6 Torr, oxygen flow 5×10^{-3} mol/sec, axial distance 12 inches from discharge nozzle, radial distance from stream axis to sample 0.75 inches, maximum film temperature 80°C, and exposure time 900 seconds. The discharged gas contained 3 to 4% oxygen atoms at these conditions, as determined by light titration techniques.¹⁴

RESULTS

Reactor Parameters. A direct proportionality between weight loss and exposure time is shown in Figure 1 for polypropylene samples exposed under the conditions described earlier. The weight loss was also proportional to electric discharge power as shown in Figure 2. The intensity of the visually-observed afterglow¹⁴ was in qualitative agreement with the observed variation of weight loss. This was also true for the variation in afterglow downstream. Figure 3 shows that the effect of the stream on sample weight loss decreased as one proceeded further downstream from the nozzle exit. As the sample was moved from the center of the exhaust stream outward, the weight loss decreased rapidly and then leveled off. The leveling off at the wall boundary is consistent with the observation that the glow downstream of the discharge exit filled the whole tube, of 1.5 inches in diameter. No significance should be placed on the fact that the sample weight loss within this region decayed and was not flat, because the large structure of the sample holder would have destroyed any local atom distribution across the stream.

In the absence of electrical discharge or when oxygen was replaced by helium, no significant weight changes in the sample were observed. No significant deviation in the transmission of infrared spectra of the treated and control samples, was resolvable on a Beckman IR5 Spectrophotometer.

The results for the weight change and the scratch, peel strength and surface wetting tests for polyethylene, polypropylene,

polyvinyl fluoride, polyethylene terephthalate, polytetrafluoroethylene, and polytrifluorochloroethylene films exposed to the oxygen plasmastream are shown in Table I.

A rather good correlation is observed between the weight loss for polymers, upon exposure, with the scratch test, which is a measure of the strength of the substrate bond with inks and lacquers. Correlation with the other two properties, however, is not so clear. In the peel strength test, it is interesting to note that polypropylene has a greater strength than polyethylene before treatment, and is not essentially affected, while for polyethylene, a large change -- about three -- is effected. However, the opposite result is experienced when comparing polyethylene and polypropylene for the surface wetting test, *i.e.*, polypropylene is more affected. The surface wetting is most effective for the polyester and then, surprisingly, there is a large effect for the polytrifluorochloroethylene. In general, one might conclude from this table that the less stable hydrocarbon polymers of ethylene and propylene are relatively reactive to the oxygen stream, while the perfluorocarbon and perfluorochlorocarbon polymers are virtually inert, except for surface wetting. An intermediate order of reactivity is shown by the moderately stable and polar polyvinyl fluoride and polyethylene terephthalate (polyester).

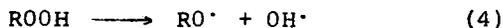
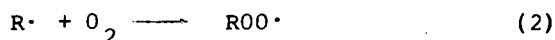
It is interesting to speculate on the effectiveness of the oxygen atoms in the stream for reacting with the surface. If we assume the oxygen atom reacts with a CH_2 group, we can then calculate the effectiveness of the stream by computing the number of oxygen atoms striking a CH_2 group on the surface. If we assume a surface cross-section for the CH_2 group in polyethylene of $25 \times 10^{16} \text{ cm}^2$, from the number of oxygen atoms which strike the surface under the experimental conditions, 6×10^{19} per $\text{cm}^2 \text{ sec}$, and from the observed weight loss, assuming the CH_2 group is removed from the surface, 2×10^{15} CH_2 groups per $\text{cm}^2 \text{ sec}$, will be removed. This means that about one in 10^4 oxygen atom collisions with the surface is effective. These numbers indicate that several monolayers of CH_2 surface are removed per second, which is difficult to rationalize with the observation in Table I that surface properties change considerably from one to 900 seconds.

DISCUSSION

Corona Discharge and Thermal Oxidations. Polyethylene film placed directly in a corona discharge of oxygen at one atmosphere has been shown to experience a loss in weight which is directly proportional to the time of exposure, and to gain weight when placed just below the discharge.¹⁵ Cooper and Prober related the formation of oxygenated surface products to reactions of the ozone (formed in the discharge) with double bonds of unsaturated polyethylene molecules. They ascribed the loss in weight of the polymer placed directly in the discharge to other reactions involving either electron or atom attack on the polymers, their data being inconclusive for a choice of mechanisms.

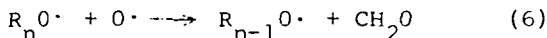
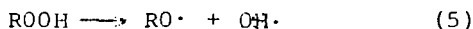
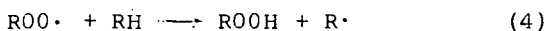
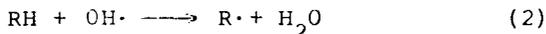
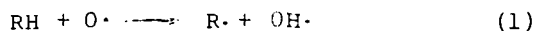
The present plasma work establishes that atom attack of the polymer is indeed a possible mechanism for surface reaction in the corona discharge although it does not rule out the possibility of other mechanisms.

Turning from corona discharge to thermally-induced oxidation of polyethylene and related compounds, the following simplified sequence of initial reactions has been discussed by Luongo¹⁶ and Grassie¹⁷



Plasmajet Oxidations. The data presented in this paper can be accounted for by the assumption of reaction of oxygen atoms with polymer to form oxygenated macromolecules which ultimately, through chain scission reactions, form products of lower molecular weight and higher vapor pressure. These volatilize and continuously expose fresh polymer surface. At steady-state conditions, an appreciable concentration of oxygenated macromolecular species must remain on this "fresh" polypropylene surface. The relatively polar oxygenated sites introduced on the polymer are responsible for the change in the surface properties of the treated samples shown by the data for the scratch, peel strength and wetting tests in Table I.

A possible series of reactions for the surface oxidation of polymer in the oxygen plasmajet is given below:



The collision of an oxygen atom with polymer initiates reaction as shown in steps (1) and (2). These free radical steps are unlike thermal initiation, in which energy must be supplied to the polymer.^{17,18} Steps (3) through (5), identical with the thermal sequence, show reactions of the undissociated oxygen (from the gas phase) with the surface polymer radicals. Degradation of polymer molecules by oxygen atoms is shown in step 6 to lead smaller radicals. These smaller radicals may sublime from the surface accounting for the weight loss. The surface recombination of polymer radicals is shown in step (7). Oxidation reactions may continue in the gas phase. Where chain termination steps such as (7) control the rate at which the polymer is degraded, the overall rate with respect to polymer consumption at a given free radical concentration can be expected to be constant with time in agreement with the data of Fig. 1.

COMMERCIAL CONSIDERATIONS

In corona discharge processes, the exact geometry and electrode separation as well as the composition and shape of the material treated can be expected to be of critical importance. Corona discharges concentrate at physical defects (pinholes, voids, and conductive occlusions) in polymers and rapidly enlarge them by electrical breakdown.⁷ In the nonequilibrium plasmajet process, the isolation of the discharge from the material treated

will make these factors relatively unimportant. The technique described in the paper has been experimentally used to treat small cubes, cylinders, partly-metallized films, and even textiles of polypropylene. There was no observed alteration of the physical integrity of the objects.

Cost estimations show the proposed plasmajet process to be competitive with corona discharge processes for polymer surface activation.

SUMMARY

A nonequilibrium plasmajet process for activation of polymer surfaces has been developed. A stream of oxygen is partially dissociated by a glow discharge, expanded to high velocity through an orifice into a region of lower pressure and impinged on the desired surface. Parameters measured before and after treatment of a variety of polymers include weight, surface bonding characteristics, and wettability. The weight loss of the polymer increases with exposure time, discharge power, and proximity to the atom source. In general, there is a correlation between the weight loss and the surface properties.

ACKNOWLEDGMENT

This research was sponsored by the Pfaunder Permutit Corporation. The authors gratefully acknowledge the contributions to this research of Mrs. H. F. Calcote, A. Fontijn, E. E. Rosner, S. C. Kurzius, and many other persons of the AeroChem Research Laboratories, Inc.

REFERENCES

1. Staff Article; Chem. & Eng. News 40, 30 (1962).
2. Horton, P.V.; U.S. 2,658,134 (1954).
3. Wolinski, L. E.; U.S. 2,715,075-6 (1955).
4. Kreidl, W. H. and Hartman, F.; *Plastics Tech.* 1, 31 (1955).
5. Kritchevar, M. F.; U.S. 2,648,097 (1957).
6. Traver, G. W.; B. P. 771,234 (1953).
7. Oliphant, Murray, Jr.; *Insulation* 9, 33 (1963).
8. Patent Applications on the process have been filed.
9. Rosner, L.E. and Calcote, H.F., AeroChem TM-10 October 1958; ASTIA AD 207 590.
10. Fontijn, A., Rosner D.E., Kurzius, S.C., *Can. J. Chem.* (submitted).
11. Wechsberg, L. E., and Webber, J.B.; *Soc. Plastics Eng. Tech. Papers* 5, 846 (1959).
12. McLaughlin, T.F.; *Soc. Plastics Eng. Tech. Papers* 6, 37 (1960).
13. Allan, A. J. G.; *J. Polymer Science* 38, 297 (1959).
14. Kaufman, F.; *Proc. Roy. Soc. A* 247, 123 (1958).
15. Cooper, Glenn D. & Prober, Maurice; *J. Polymer Science* 44, 397 (1960).
16. Luongo, J. P.; *J. Polymer Science* 42, 139 (1960).
17. Grassie, N.; Chemistry of High Polymer Degradation Processes, Butterworths Publications, Ltd., London, England (1956).

TABLE I

EFFECTS OF NONEQUILIBRIUM OXYGEN STREAM
ON POLYMER SURFACE PROPERTIES

TEST	Scratch, Numerical Rating ^a	Peel Strength, grams/inch	Surface Wetting, degrees tilt	Weight Loss, mg/sample ^b
TIME, sec	1 900	0 1 900	0 1 900	900
Polyethylene	2.7 3.0	360 420 1000	35 38 51	3.8
Polypropylene	3.0 3.0	1400 1350 1300	16 52 42	3.7
Polyvinylfluoride	2.0 2.5	100 120 200	23 38 23	3.4
Polyester	1.2 2.1	200 290 520	41 13 12	1.1
Polytetrafluoro- ethylene	1.0 1.5	66 50 54	25 33 39	0
Polytrifluoro- chloroethylene	1.5 1.5	210 220 200	20 36 53	0

a. Ratings 1 - 3 correspond to no change to great change.

b. 7.06 in² of surface area per sample were used.

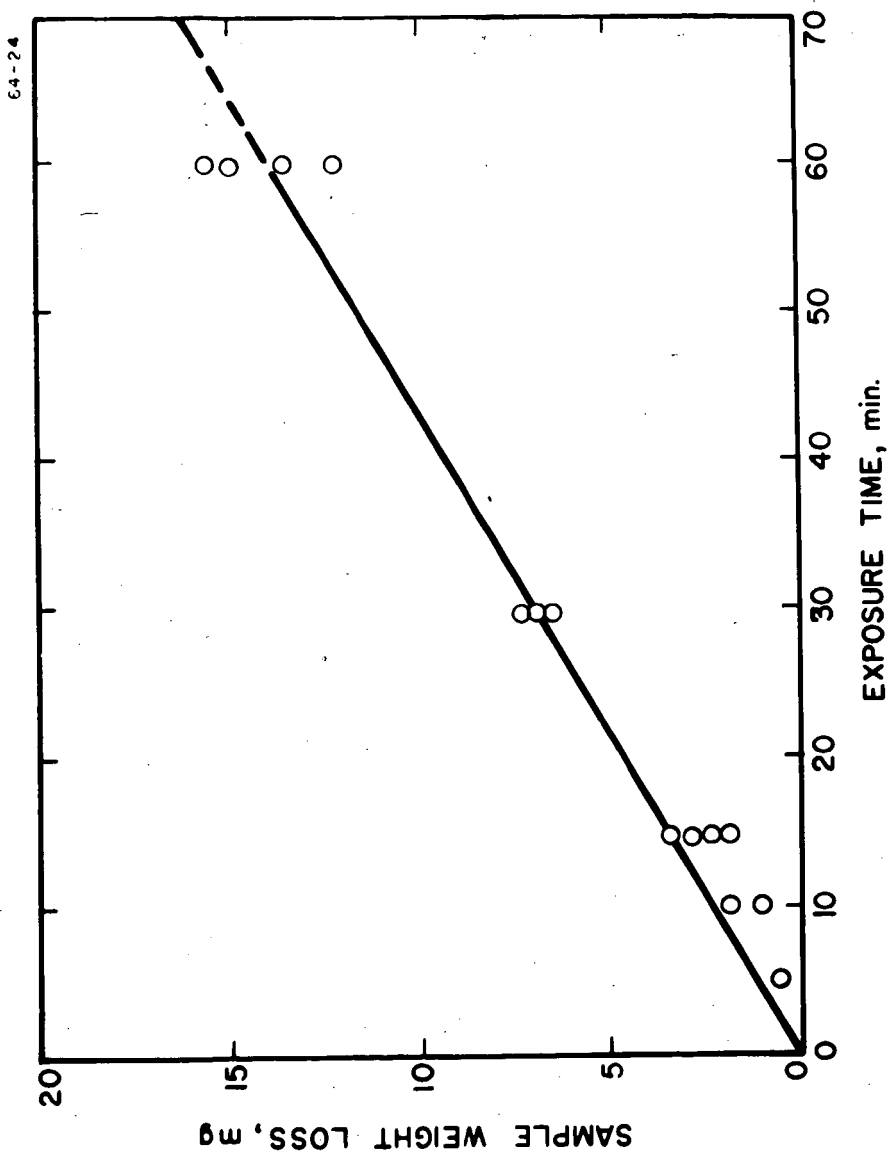


FIG. 1 THE INFLUENCE OF EXPOSURE TIME ON THE WEIGHT LOSS OF POLYPROPYLENE

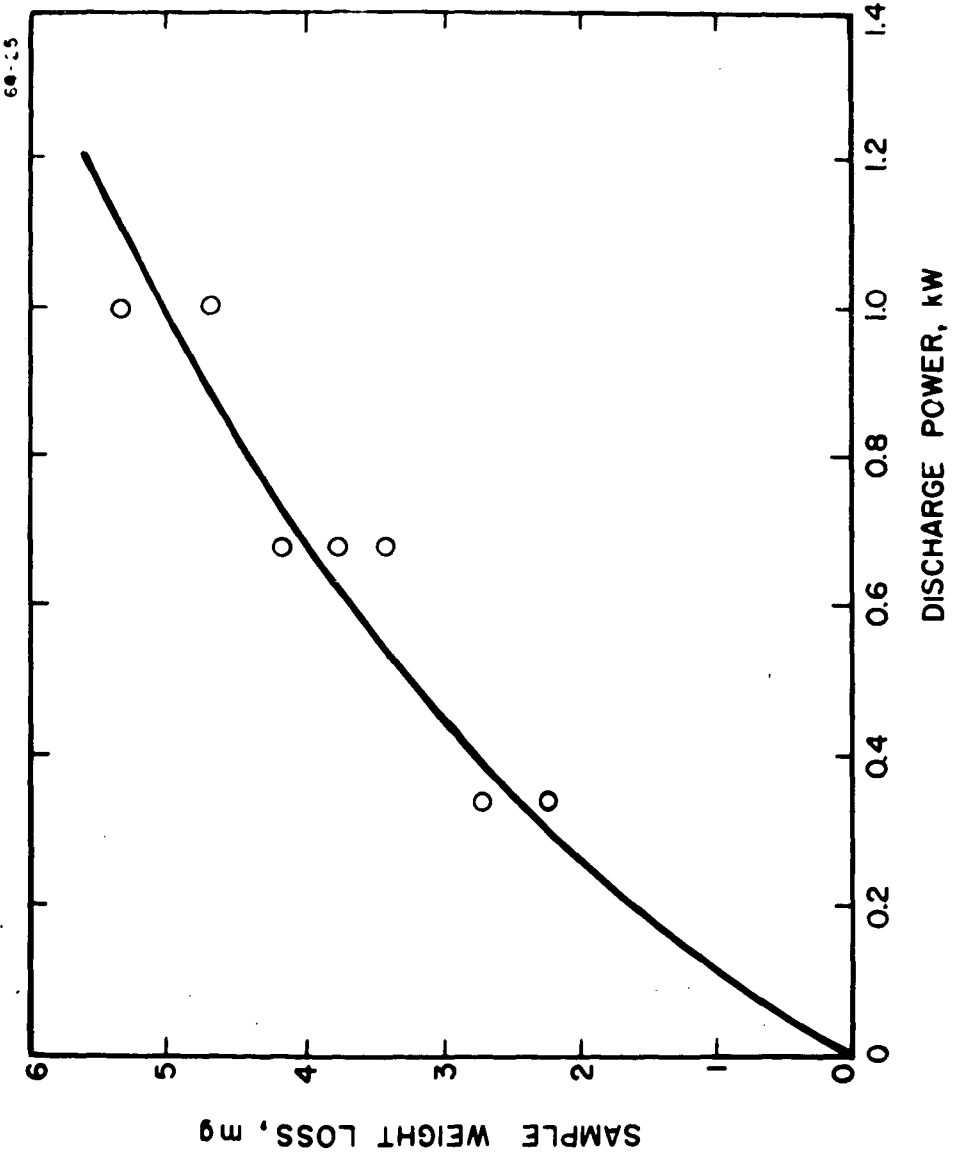


FIG. 2 THE INFLUENCE OF DISCHARGE ELECTRIC POWER ON THE WEIGHT LOSS OF POLYPROPYLENE

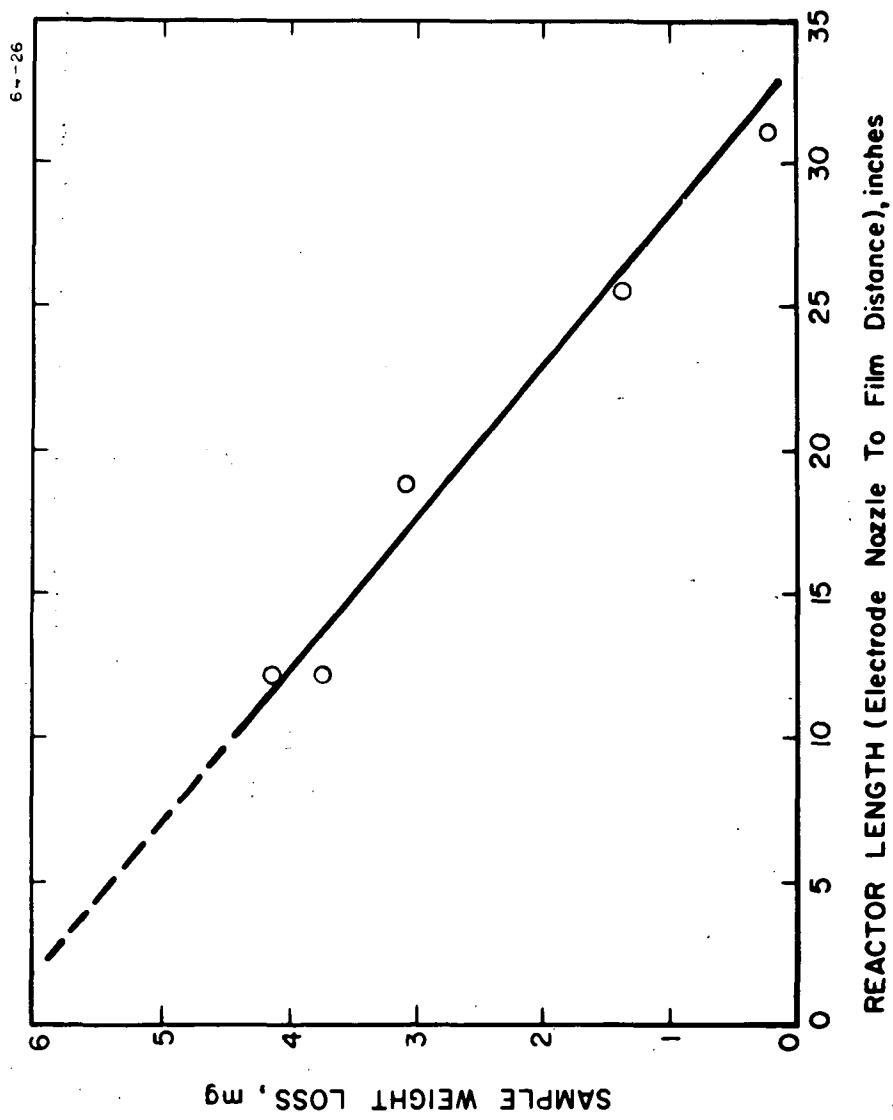


FIG. 3 THE INFLUENCE OF REACTOR LENGTH ON THE WEIGHT LOSS OF POLYPROPYLENE

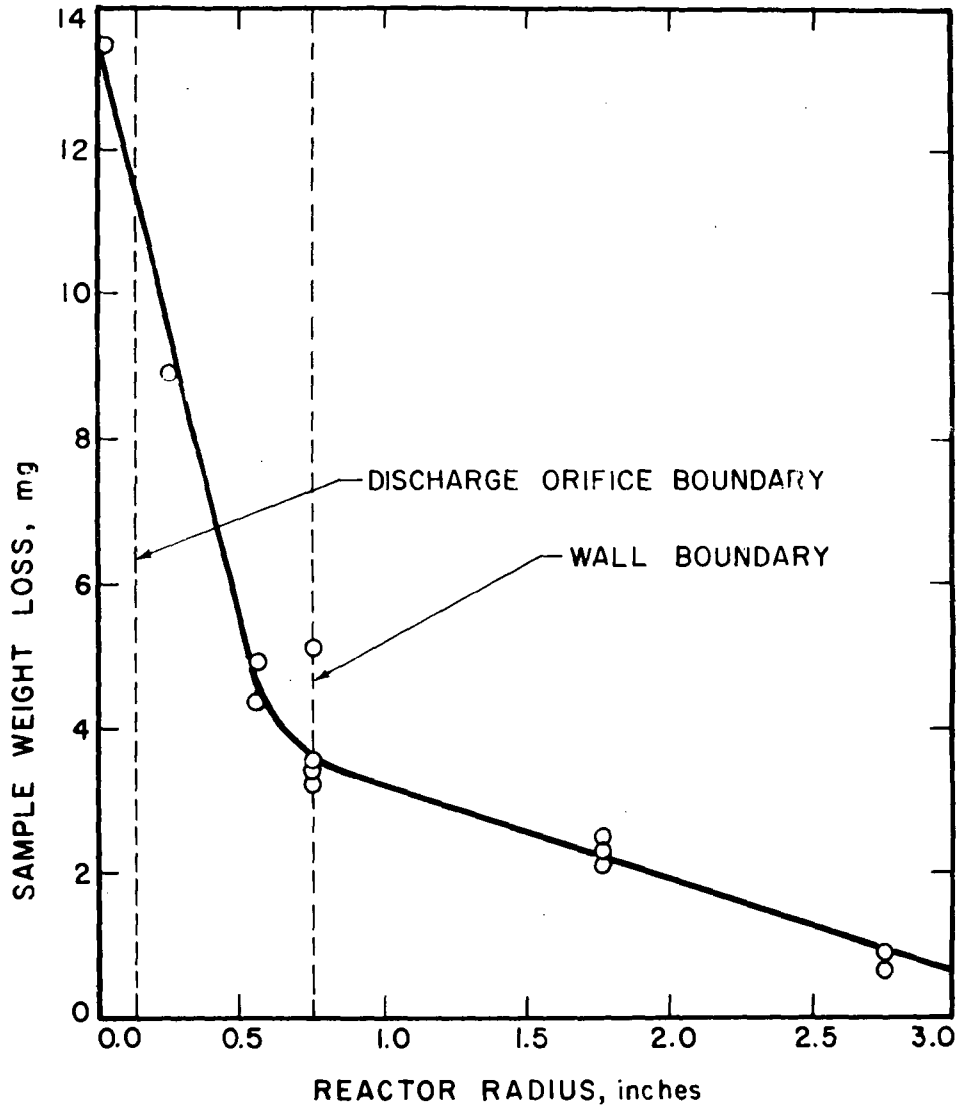


FIG. 4 THE INFLUENCE OF RADIAL DISTANCE ON THE WEIGHT LOSS OF POLYPROPYLENE

Interaction of Materials and Plasmas:
Spectroscopic Studies of Chemical Phenomena

L. Isaacson, T. Wentink Jr., G.J. Economou

Avco Corporation
Research and Advanced Development Division
Wilmington, Massachusetts

I. Introduction

Webster defines ablation as a removal or a carrying away. Thus, the ablation process, as applied to materials, denotes the removal or carrying away of material. To study this process, arc jets or plasma jets have been employed as sources to "ablate" samples. Reported here are the results from using various configurations of commercially available plastics. Surface characteristics (e.g., surface temperature, emissivities, and absence or presence of char formation and removal) and plasma interaction (e.g., the formation of gaseous degradation products) have been studied. To accomplish this, emission spectroscopic and spectrographic techniques were employed over the wavelength range 0.2-9.0 μ . Results of measurements on Delrin*, $(-\text{CH}_2-\text{O}-)_x$, Zelux, $(-\text{C}_6\text{H}_4-)_x$, $\text{C}(\text{CH}_3)_2-\text{C}_6\text{H}_4-\text{O}-(\text{C}=\text{O})-\text{O}-)_x$, and to some extent Teflon, $(-\text{CF}_2-\text{CF}_2-)_x$, will be cited as illustrative examples.

When heat is applied (in this case from the arc jet), the surface temperature of the materials rises until at some point the ablation process, and not the heating process, becomes the dominant mechanism controlling the chemistry. However, this ablation process can occur in several ways. First, a pseudosublimation may take place at the surface; namely, degradation of the polymer to gaseous products with no resulting surface changes; second, degradation of the polymer which leads to a change to the liquid state with subsequent flowing away of the liquid phase; and third, degradation of the polymer yielding some type of a char which either forms and blows off, or adheres to the model surface. Combinations of the above may also take place. Examples of the various types of ablators are graphite, quartz and Zelux respectively. A good discussion of ablation is given in reference 1.

II. Plasma Jet Characteristics

For the polymeric materials used, the heat inputs (enthalpies) and heat fluxes from the various plasma jets are more than enough to cause ablation to be

*Delrin is the DuPont trade name for Polyoxymethylene, the Celanese Corp. produces this material under the tradename Celcon. Lexan is a commercially available polymer resin which in the final, fabricated form is known as the plastic Zelux.

¹M.C. Adams, ARS J., 29, 625 (1959).

the dominant decomposition mechanism. One type of plasma jet employed is of the same type as that described by Watson, Ferguson, and Nicholls.² Another type is similar except that a plenum chamber (for adding gas downstream and thus being able to produce simulated air) was used. The electrodes are of the noneroding type (a copper anode and a thoriated tungsten cathode).

Although the plasma jets are not in complete thermal equilibrium, the approach to equilibrium is much closer here than in glow discharges at the same pressure.

With nitrogen as the propellant gas, the arc power was of the order of 25 kw while the enthalpy (H/RT) was 220 (7392 Btu/lb).

III. Experimental Techniques

It is possible, with infrared techniques, to follow the surface behavior of plastic materials when they are subjected to the plasma jets by determining surface temperatures as a function of time, and surface temperature and emissivity as a function of wavelength. Dramatic changes in surface temperature will also give an indication of char formation and propagation. To carry out these measurements, a CaF₂ or NaCl prism was used in a Littrow configuration which was coupled with a Au-doped Ge detector chopped at 690 cps. The spectra or other traces were displayed on a Tektronix Type 502 oscilloscope by sweeping the scope at the desired rate. For time histories, the wavelength is kept fixed. For spectral scans, the Littrow mount is driven by a cam which oscillates the mount and scans the desired $\Delta\lambda$ every 0.2 second. For wavelength calibration, a helipot is attached to the Littrow arm and a periodic wave is displayed on one beam of a dual-beam oscilloscope; the signal output is displayed on the other. A Barnes black-body is used to give absolute temperature calibration.

For all visible and ultraviolet results, the spectra were recorded photographically on a Hilger E498 (all quartz) or E528 (quartz and glass employing quartz optics) using Kodak 103-F plates. The F plates were used because the widest wavelength coverage (0.23 to 0.70 μ) could be obtained without serious loss of sensitivity.

The IR gaseous spectra (0.8 to 1.5 μ) were taken with a single pass monochromator employing an SiO₂ prism and PbS detector and were recorded on a dual-beam oscilloscope (signal output on one beam and drum number readings on the other).

IV. Surface Characteristics

Figure 1 is the room temperature absorption spectrum of Delrin, while figure 2 is the emission spectrum (2 to 7 μ) for a Delrin sample ablating in a nitrogen plasma jet. Note the strong absorption and emission in the 3.3 μ region and beyond 7 μ while there is weaker absorption and emission in the 4.0 to 6.5 μ regions. Thus, from figure 2, we have determined the surface temperature of Delrin at $\lambda = 3.3\mu$ to be $725 \pm 10^\circ\text{K}$. The approach used to deduce the surface

²M.D. Watson, H.I.S. Ferguson, R.W. Nicholls, Can J. Phys., 14, 1405 (1963).

temperature was to compare the absolute radiant emittance obtained with that from a calibrated blackbody in a spectral region where the assumption of the emissivity, ϵ , near unity is valid. This assumption in turn, is based on transmission measurements of absorption spectra of thin films to determine the wavelengths where the absorptivity is so large that the emissivity also must be near one; i. e., Kirchoff's Law is invoked. This assumption of near unit emissivity is most uncertain in the case of charred materials where often the reflectivity can be high in the infrared.

With a heavy char former such as Zelux, the surface temperature varies quite widely with time, so in order to watch this behavior a constant wavelength is picked and the behavior is scanned as a function of time. Figure 3 gives the IR emission from ablating Delrin and figure 4 gives the IR emission from ablating Zelux; both taken at $\lambda = 3.4\mu$. The big difference between the heavy char former (Zelux) and the non-char former (Delrin) is readily apparent when the two figures are compared. The spikes in figure 4 show the super-heating and blowing off of the char layer.

Figure 3 will also illustrate another point. Note that in the beginning (up to 1/2 second) the voltage rises very rapidly and then changes slope. We have called this point the "breakpoint" and ascribe it as the point where the rate of ablation has become large enough to control the surface temperature. For a number of materials, the breakpoint temperature obtained from these plasma jet measurements has been correlated with those obtained from thermogravimetric analysis (TGA) decomposition experiments. One such experiment for Delrin in air is illustrated in figure 5. For Delrin, we measure the breakpoint temperature as $593 \pm 10^\circ\text{K}$, and from TGA, the temperature for 100 percent decomposition is 605°K . Because of char formation, the heavy char formers do not usually yield a well defined breakpoint (note figure 4).

V. Gaseous Products

The sample configurations used to date to obtain gaseous spectra are pipes and cones. The pipes are 4-1/2 inches long and 2 inches in diameter. The hole through which the gas flows is initially 1 inch in diameter. Because of the nature of the jet, the flow through the pipe is laminar. The cones employed have 1-inch base diameters and an included angle of 20 degrees. When the plasma interacts with the cone, a shock wave is set up and the region between the shock envelope and the surface consists of high temperature gas highly contaminated with ablation products, and as an emission source has considerable intensity.

Figures 6, 7, and 8 are spectra of a Zelux pipe in a Helium jet, a Zelux pipe in a nitrogen jet, and a Zelux cone in a nitrogen jet, respectively. Table I is a compilation of the species identified as present and illustrates the effect of a change in the plasma gas and in the sample configuration. The helium plasma jet produces a hotter jet (higher gas temperature) than the nitrogen jet while the effect of a higher temperature due to shock wave effects can be seen by comparing figures 7 and 8.

A close examination of figure 8 shows that three of the dominant radiating species in the visible are CN, CH, C₂. Kokline³ firing preheated Zelux models at 16,000 ft/sec in a ballistic range also finds the three predominant visible radiators as CN, CH and C₂. Thus, although two widely different experimental media have been used, under the proper conditions there is correlation in the results obtained. In this way, one sees that plasma jet results can point the way to, and act as, a starting point for more sophisticated experiments. One such experimental medium is the shock tube. In noting the various species that are formed during degradation of a plastic in a plasma jet, mixtures of gases which, when shocked, will yield the appropriate species, can then be studied by simultaneously monitoring the important wavelengths. With a drum camera, it would be possible to monitor variations in the behavior of some species in the visible region. One advantage of the plasma jet is the large test time one has when compared with ballistic ranges and shock tubes.

Infrared measurements in the 0.8 to 2.0 micron region showed strong gas radiation characteristic of the CN red system when a Zelux model ablated in a nitrogen arc. A similar scan of the nitrogen jet without any model produces the first positive system of nitrogen, but at a much lower intensity level.

Figure 9 is the spectrum obtained when a Teflon model ablates in an Argon plasma jet. The principal diatomic, UV radiator is CF along with some continuum radiation. The CF spectrum that is produced is quite pure and avoids many of the impurities (e.g., CF₂, S) encountered by other investigators. The relatively short test times needed to obtain decent intensity compared with other methods (e.g., flames) is well illustrated. Thus, by picking the proper material and arc gas, one can obtain and study, relatively easily, high temperature diatomic species.

VI. Acknowledgment

The work reported in this paper was supported by contracts with the Air Force Ballistic Systems Division (AFBSD) of the Air Force Systems Command.

The authors acknowledge with appreciation the advice and help of many individuals at RAD during the course of this work and to Dr. T. Marshall for reading and commenting on this manuscript.

³A. Dmitrieff-Kokline, Spectrographic Studies of the Radiation Emitted by Hypersonic Projectiles, Canadian Armament Research and Development Establishment, TN-1564, May, 1963.

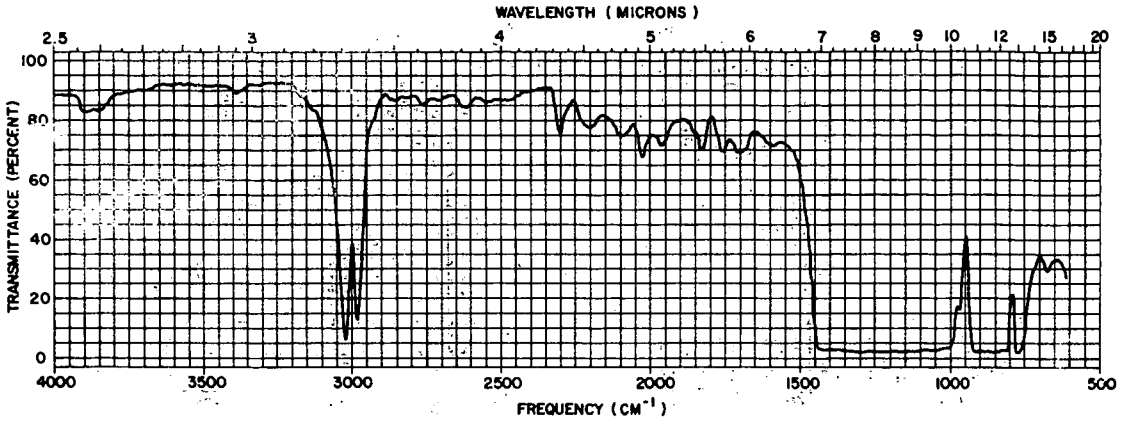
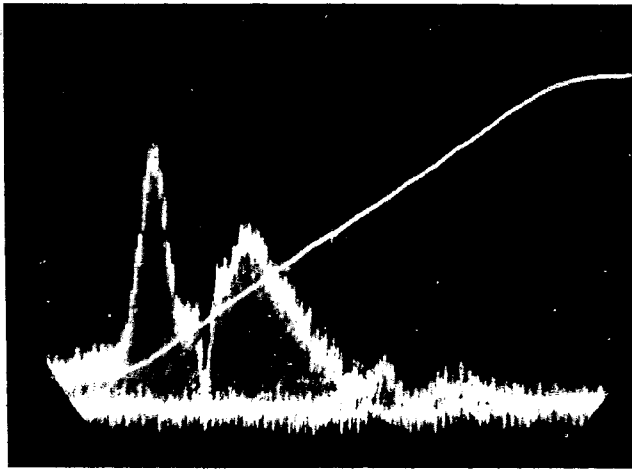
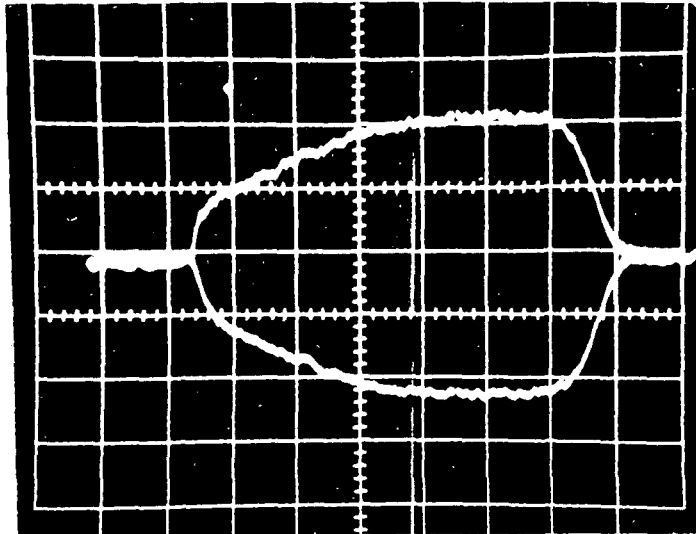


Figure 1 ROOM-TEMPERATURE INFRARED ABSORPTION SPECTRUM OF DELRIN (0.003-inch Film)

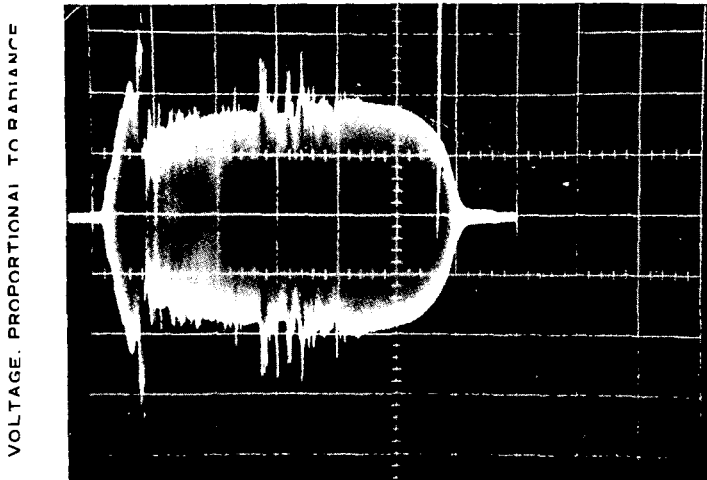


3.0 3.4 4.3 4.9 6.2 7.5 μ
 CO₂ H₂O null

Figure 2 DELRIN INFRARED EMISSION SPECTRUM (0.5 V/cm)



($\lambda = 3.4$ MICRONS)



64-1245

Figure 4 INFRARED EMISSION HISTORY OF ABLATING ZELUX
($\lambda = 3.4$ MICRONS, 5 SEC/CM SWEEP)

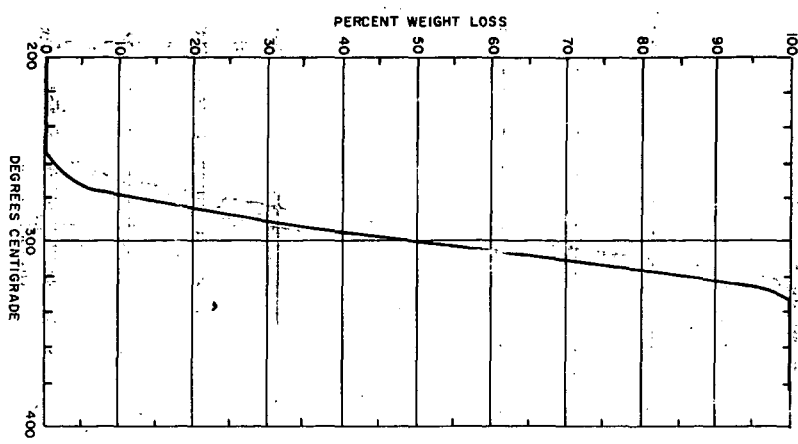
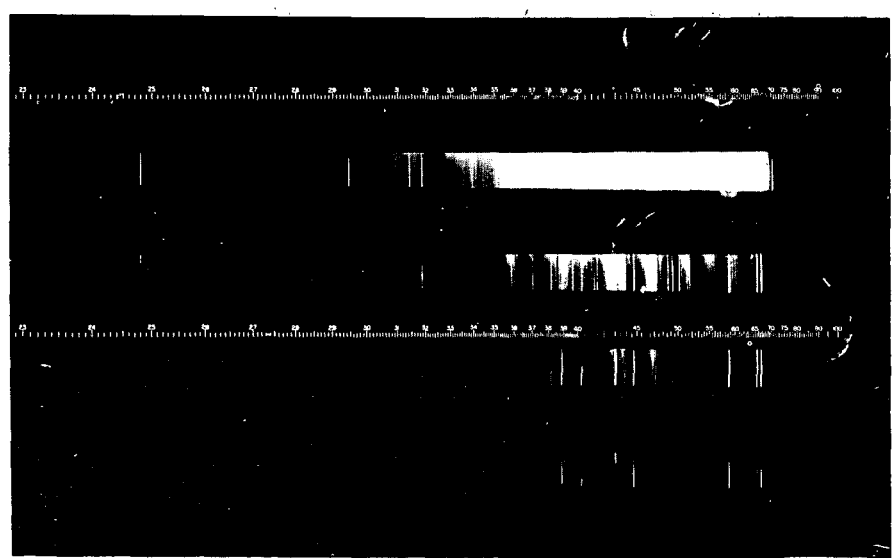


Figure 5 THERMOGRAVIMETRIC ANALYSIS, DELRIN IN AIR

ZELUX PIPE/HELIUM
2300 A

- a NO ARC SPECTRUM
- b Sw, 10 SECONDS
- c Sw, 1 SECOND
- d Sw, 1/5 SECOND
- e Sw, 1/25 SECOND



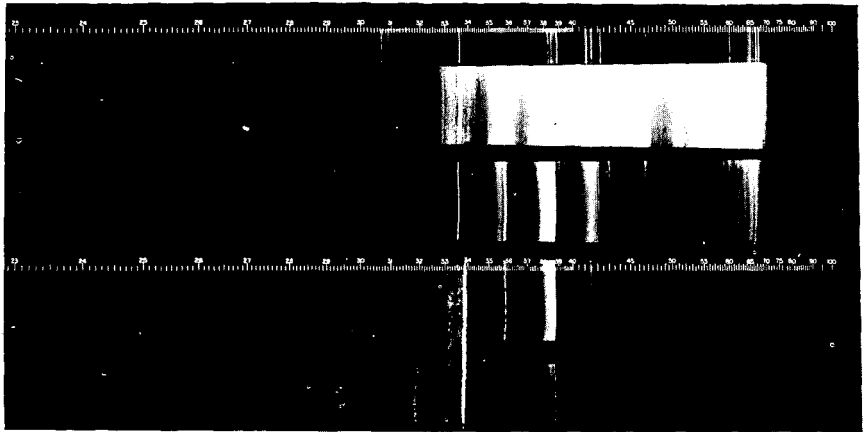
Sw = 60-micron slit
EXPOSURE TIMES AS GIVEN ; a PLUME ONLY ;
b THROUGH e WITH MODEL IN STREAM

63-7171

Figure 6 ZELUX PIPE -- HELIUM

ZELUX PIPE / NITROGEN
2300A

- a Sw, 10 SECONDS
- b Sw, 10 SECONDS
- c Sw, 1 SECOND
- d Sw, 1/5 SECOND
- e Sw, 1/25 SECOND

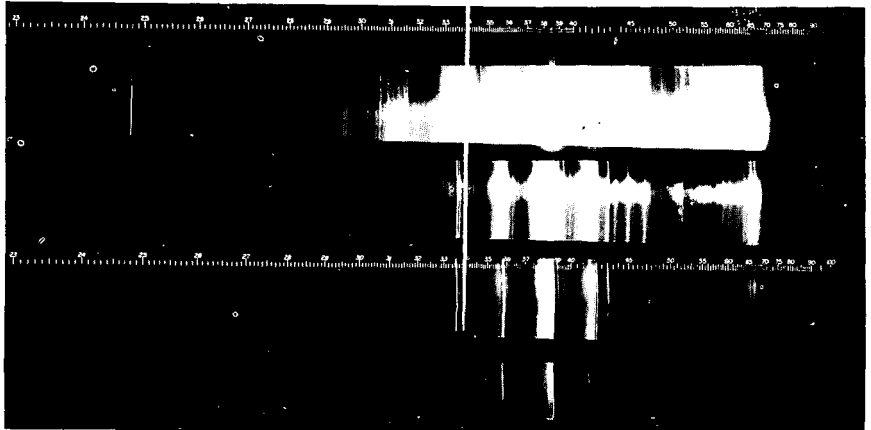


Sw = 60-MICRON SLIT
EXPOSURE TIMES AS GIVE; a PLUME ONLY;
b THROUGH e WITH MODEL IN STREAM

Figure 7 ZELUX PIPE -- NITROGEN

ZELUX CONE / NITROGEN
2300A

- a Sw, 1 SECOND
- b Sw, 10 SECONDS
- c Sw, 1 SECOND
- d Sw, 1/5 SECOND
- e Sw, 1/25 SECOND

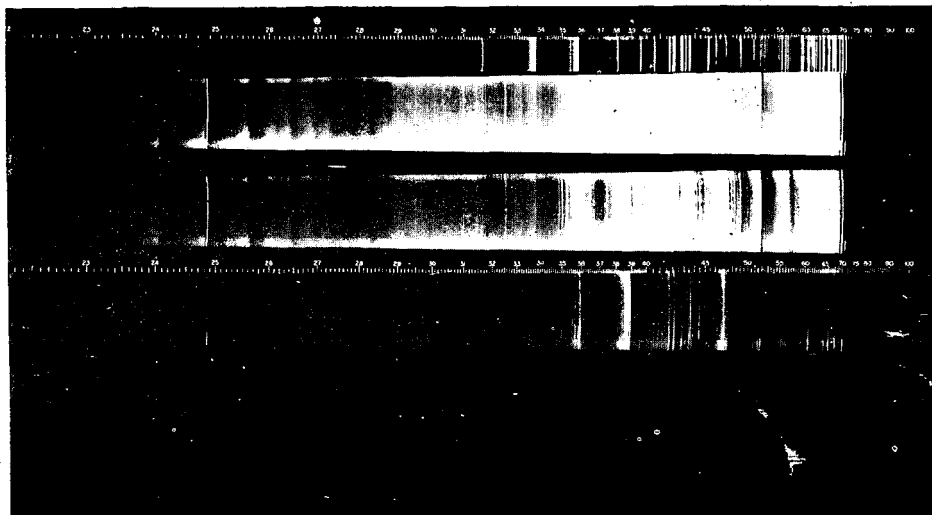


Sw = 60-MICRON SLIT
EXPOSURE TIMES AS GIVE; a PLUME ONLY;
b THROUGH e WITH MODEL IN STREAM

Figure 8 ZELUX CONE -- NITROGEN

TEFLON CONE / ARGON
2200 A

- a. Sw, 10 SECONDS
b. Sw, 20 SECONDS
c. Sw, 10 SECONDS
d. Sw, 1 SECOND
e. Sw, 1/5 SECOND



Sw = 60 micron slit
EXPOSURE TIMES AS GIVEN; a PLUME ONLY;
b THROUGH e WITH MODEL IN STREAM

Figure 9 TEFLON CONE -- ARGON

TABLE I

SPECIES IDENTIFIED IN SPECTRA OF ZELUX-CONTAMINATED GASES

ZE Pipe/He (Figure 2)	ZE Pipe/N ₂ (Figure 3)	ZE Cone/N ₂ (Figure 4)
C (s) ^a	C (m)	C (s)
H (s)	H (w)	H (m)
-	CN (s)	CN (s)
CH (m)	CH (m)	CH (m)
C ₂ ^b (m)	C ₂ (m)	C ₂ (m)
-	NH (m-w)	NH (s)

a: s = strong, m = medium, w = weak mean relative intensities from visual estimates of spectral plates.

b: Besides the C₂ Swan systems that are identified, the following C₂ systems (with bandhead values) also are identified as present when ZE pipe is in a helium plasma jet: Fox-Hersberg (heads at 2855, 2987, 3129, and 3283 Å), Deslandres-D'Azambula (heads at 3400, 3588, 3607, 3850, 4040, 4060, and 4100 Å).